MICROBIAL FUEL CELLS: DESIGN, CONTROL-ORIENTED MODELING, AND EXPERIMENTAL RESULTS

By

Ali Abul

A THESIS

Submitted to
Michigan State University
in partial fulfillment of the requirements
for the degree of

Mechanical Engineering - Master of Science

2015

ABSTRACT

MICROBIAL FUEL CELLS: DESIGN, CONTROL-ORIENTED MODELING, AND EXPERIMENTAL RESULTS

By

Ali Abul

There is no doubt about how crucial to have sustainable energy in this era. Researchers focus on fuel cells because of their high efficiency, environmental friendliness, and independence from limited sources, etc. Microbial fuel cell (MFC) is a promising technology that responds to the demand of sustainable energy. MFCs, similar to other fuel cells, use catalysts and produce electricity through chemical reactions during substrate break-down. In this case, MFCs use bacteria as the catalysts to break down the organic matter.

There have been control studies on fuel cells, specifically on hydrogen fuel cells, for various purposes. Because MFCs are still not well understood, similar control studies have not been adequately conducted. In this study, a control-oriented mathematical model for MFC dynamics is developed and analyzed. An MFC system is designed and developed, which has successfully demonstrated production of electricity. Experiments are conducted to identify the model parameters and validate the model. For the MFC prototype, *G. sulfurreducens* strain PCA is used as the pure bacteria culture with the acetate as the substrate. The MFC used in this study adopts a membrane-less single-chamber configuration, and utilizes an air-cathode and a carbon-brush anode.

Once the model is developed, the behavior of an MFC is analyzed using system theory. In particular, the equilibria of the system in the continuous mode, where the MFC is fed with the substrate at a constant rate are computed. Furthermore, Jacobian analysis and phase portraits are used to understand the stability properties of the equilibria.

To my dearest parents Zeynep and Mehmet Resit Abul, my lovely wife Stephanie Ann Duperon, my supportive siblings Berat and Meral Abul.

ACKNOWLEDGMENTS

This research was supported in part by the National Science Foundation (IIS 1319602). I am most grateful to my advisor, the director of Smart Microsystems Lab at Michigan State University, Prof. Xiaobo Tan. Through my entire study Prof. Tan guided me wisely with his extensive experience and knowledge. Prof. Tan encouraged me to be a researcher but also prepared me for becoming an engineer with different knowledge and skills from multiple disciplines. His valuable guidance and generous encouragement benefited me a lot in my research and will continue to benefit my future career.

I want to thank my committee members: Prof. Hassan Khalil and Prof. Guoming Zhu at Michigan State University, for joining my advisory committee and offering me insightful comments. Their extensive knowledge and guidance improved the quality of my research.

In this study, Prof. Gemma Reguera and her lab members providedimmense help during my prototyping effort and experiments. I am specifically indebted to Dr. Rebecca Steidl, who gave me useful comments on my system and met most (if not all) of my needs in the experimental part of this study.

I am very grateful to my lab members. We brainstormed for each other's endless problems and had fun working together. Special thanks go to John Thon, Osama Ennasr, Hong Lei and Jun Zhang, who directly contributed to my research. I would also like to thank staff members in the ECE department, especially Brian Wright, Gregg Mulder and Roxanne Peacock. Dr. Reza Loloee generously let me use the equipment in his lab for my materials fabrication, which was greatly appreciated. I want to give special thanks to Prof. Bruce Rittmann, Prof. Bruce Logan, and Prof. Andrew Marcus who answered my questions patiently through my research.

I would like to thank my family: my parents, my mother-in-law, my father-in-law, my brother, and my sister for supporting me spiritually throughout my thesis research and throughout my life in general. Your prayer for me was what sustained me thus far.

Last but not least, I would like to give a very special thank-you to my dearest wife, who supported me throughout this study as well.

TABLE OF CONTENTS

LIST OF TABLES

LIST OF FIGURES

Chapter 1

Introduction

1.1 Background

Energy demand has always been shaping the future of technological opportunities, economy, social life and many other important areas. It is known that fossil fuels are non-renewable energy resources and contribute to various environmental issues [27]. MFCs (microbial fuel cells) are one of the potential alternatives for meeting the energy demand and they are environmentally friendly in nature [16], [18], [39], [35]. MFCs are devices that use bacteria as the catalysts to oxidize organic matter and generate current [4]. Bacteria produce electrons by breaking down organic matter and transferring the electrons to the anode (the second electron acceptor after the bacteria), and then to the cathode when the external circuit is completed. Oxygen molecules (the terminal electron acceptor) accept the electrons, which flow from the anode to the cathode. However, MFCs are still largely at the research level, and there are challenges and bottlenecks to overcome before they become commercially viable and widely adopted.

The rate at which bacteria can oxidize a substrate, and transfer electrons from the substrate to the surface of the anode has a significant effect on power generation. While having more bacteria typically means a higher oxidation rate, the concentration of bacteria could reach saturation beyond a certain level. The microorganism and substrate concentrations are the main elements in the dynamics of power generation in MFCs.

Once bacteria cover the electrode surface, they form a biofilm. It is known that as the biofilm grows thicker, mass transfer to the biofilm becomes more limiting. Therefore, current density is limited by the diffusion or advection of substrate to the biofilm. There are also limits on current and power density imposed by the internal resistance, which is related to the membrane (when present) and the materials used for anode and cathode. The voltage generated by an MFC is more complicated to understand or predict than that of a chemical fuel cell [18]. In an MFC, it takes time for the bacteria to colonize the electrode and manufacture enzymes or structures needed to transfer electrons outside the microorganism outer membrane. Furthermore, in a mixed culture, different bacteria can grow, resulting in different potentials. The potential cannot be predicted even for pure culture where there is only one type of microorganism, due to the difficulty in keeping the system 100% pure (there might be other types of microorganisms that can easily grow even when everything in the system has been sterilized). However, there are limits to the maximum voltages that can be generated based on thermodynamic relationships for the electron donor (substrates) and electron acceptor (oxidizers).

To be able to understand the phenomena behind microbial fuel cells, it is necessary to model the behaviour of bacterial substrate consumption. Despite their importance, few MFC models are present in the literature. Researchers developed models based on the microbial kinetics such as Monod kinetics, Haldane kinetics (in the presence of inhibitors) [28], and tried to understand the dynamics behind the bacterial growth and substrate concentration change, to control a chemostat based on the bacterial growth [30], [31], [32]. For MFCs, some researchers take in account the biofilm-based models, which are more detailed and provide more accurate results for cases involving microorganisms for cases that do not need mediators to give their electrons. Rittmann and McCary explained this approach in [1] with

a broad spectrum. On the other hand, there are studies where researchers use a suspended bacteria model [18], [39]. Both approaches offer acceptable comparisons with experimental results, but overall the full understanding of MFC systems is still lacking. The processes of electron transfer have been modeled before, but prior work only considered one-dimensional, multi-species model for the biofilm in the MFC [35]. Picioreanu *et al.* [47] developed a detailed 3-dimensional model for the anodic compartment biofilm. The principal aim of this model was to analyze biofilm formation and species distribution within the biofilm. This was also the first model to take into account different microbial populations competing for biofilm space and substrate. There have been studies on controlling MFCs based on the microbial dynamics [45], [38], but experimental results have not been presented to support the theoretical or numerical results.

Most MFC research focuses on maximizing power production by improving the electrode materials [55], [65], stacking of the MFCs [50], using different bacteria types [69], and exploring new designs [18]. There is not much study on the control aspect of MFCs, despite its significance on the performance of the MFC. In this research, nonlinear dynamics of an MFC is studied. A mathematical model for the MFC is constructed and verified experimentally. To be able to better understand the MFC system and to acquire data from the experiments, a single-chamber MFC system is designed and prototyped. We further characterize the equilibria of the nonlinear dynamics when the substrate is fed into the system continuously at a constant rate, and investigate the stability of these equilibria with Jacobian analysis and phase portrait.

1.2 Literature Review

1.2.1 Fuel Cells

Unlike combustion engines, fuel cells produce power with minimal pollutants, which is one of the important attractive features of fuel cells. Fuel cells produce energy from chemical reactions in contrast to combustion. However, unlike batteries, the reductant and the oxidant in fuel cells must be continuously replenished to allow continuous operation [6].

The primary components of a fuel cell are an ion-conducting electrolyte, a cathode, and an anode, as shown schematically in Fig. 1.1. Fuel cells are typically single-chambered and this chamber contains both anode and cathode components. In a typical fuel cell, hydrogen serves as the fuel to the anode and an oxidant, usually oxygen, is supplied to the cathode compartment. Hydrogen molecules are pushed into the anode where a chemical reaction breaks them down into electrons and hydrogen ions. Hydrogen ions are passed through the electrolyte and reach the cathode. On the cathode side, oxygen molecules are supplied and meet the electrons and protons coming from the anode, to form H_2O as the byproduct. There is an overall electromotive force for hydrogen and oxygen to form water as the byproduct.

The net reaction in a fuel cell is similar to the combustion of hydrogen gas, which releases the same amount of energy, except that electrical energy has been harvested instead of heat.

- Anode Reaction: $2H_2 \rightarrow 4H^+ + 4e^-$
- Cathode Reaction: $4H^+ + 4e^- + O_2 \rightarrow 2H_2O$
- Overall Reaction: $2H_2 + O_2 \rightarrow 2H_2O$ $\qquad \Delta G_{overall} = -474.4\ \text{kJmol}^{-1}$ [8].

$\Delta G_{overall}$ is the Gibbs free energy difference between reactants and products. Gibbs free energy is the energy associated with a chemical reaction that can be converted to work. The

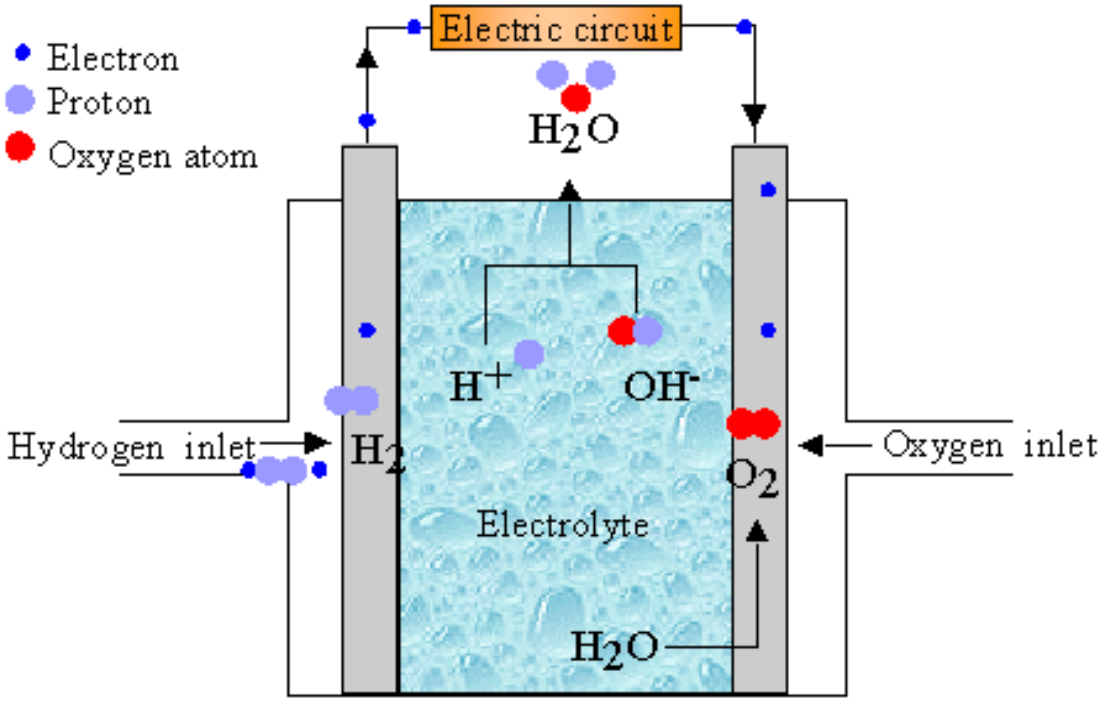

Figure 1.1 Typical fuel cell components and operation [6].

performance of a fuel cell can be measured by obtaining the polarization curve (operating curve). A polarization curve plots the voltage of the fuel cell against its current density. It can be obtained by having an adjustable external resistor and changing its value. Today, the polarization curve of a fuel cell can be obtained with a potentiostat easily. It should be done after the system reaches the steady-state open circuit potential (OCP, which is the potential when there is no current passing through the external circuit). After the system reaches the steady-state OCP, the fuel cell circuit is closed with an external resistor. By changing the resistor value slowly (waiting some time at each resistor value), one can measure the voltage across the terminals and plot the voltage-current curve.

The operating curve and the power curve together give vast amount of information about the fuel cell, such as internal resistance of the system, optimal external resistance to be used, operating voltage, maximum power, and overpotentials of the system [18]. In Fig. 1.2, the

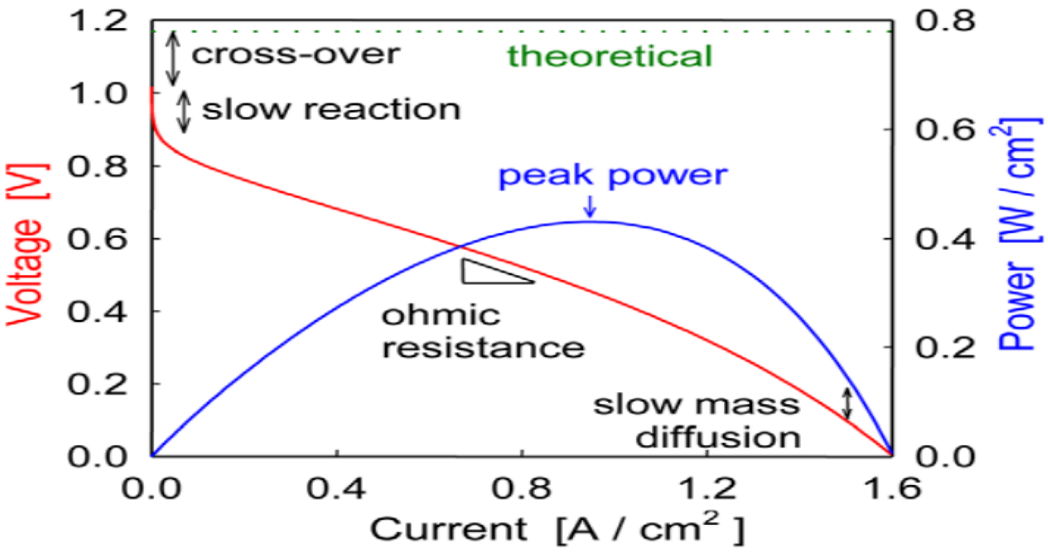

Figure 1.2 An example of the polarization curve of a fuel cell [7].

slope of the polarization curve in the linear part provides an idea of the internal resistance of the fuel cell [7]. It can be seen in Fig. 1.2 that there are three main regions for the voltage drop with the change of the current density. The theoretical OCP can be calculated from the Nernst equation [35], [18]. However, the measured OCP will be lower than this theoretical value due to cross-over. In a practical fuel cell, some fuel will diffuse from the anode through the electrolyte to the cathode whereas the it should be only ions which diffuse. This will react directly with the oxygen at the cathode, producing no current from the cell. This small amount of wasted fuel that migrates through the electrolyte is known as fuel crossover [12]. The measured OCP is always lower than the theoretical value due to,

1- Activation losses (due to activation energies and electrochemical reactions happening in the fuel cell)

2- Ohmic losses (due to resistance of the flow of ions in the electrolyte and electrode)

3- Concentration losses (due to mass transfer limitations)

As the current increases, the potential starts decreasing due to the activation losses which appear at low current values. Activation overpotentials are due to energy lost for initiating chemical reactions and the energy lost due to the electrons traveling to the terminal electron acceptor. The linear part of the operating curve is due to the ohmic losses (even though there are also some negligible activation losses occurring in this part). Ohmic losses can be the most important part for an optimum fuel cell design. These losses are usually due to the internal connections, the diffusivity of the membrane, the resistance of ion conduction, etc. Finally, the voltage decreases because of the concentration losses with the high current density. These losses are also called mass transfer losses and are due to either limitation of the concentration of reactants or oxidants in the fuel cell.

1.2.2 Microbial Fuel Cells

Microbial fuel cells have similar characteristics as other types of fuel cells except that they use the bacteria to reduce the substrate. However, comparing to most of the other fuel cells, MFCs have additional benefits. While giving useful electricity, bacteria also treat wastewater (if used as the substrate) by breaking down the organic matter in wastewater. Most fuel cells rely on expensive catalyst materials whereas that occurs naturally by microorganisms in MFCs. Hydrogen fuel cells require complex control systems since they need to use highly regulated storage and distribution systems. MFCs can use a wide range of organic matter as the substrate and can utilize microorganisms that are commonly used and can easily be found in natural environments. MFCs can also be operated at room temperature unlike the most common fuel cells, which require high temperature and expensive control systems for that. One MFC unit (either single or double-chambered) might have a low voltage output (less than 0.3 V), so MFCs can be stacked to increase the total voltage output.

1.2.2.1 MFC Working Principle

As can be seen in Fig. 1.3, there are two half-chemical reactions occurring in an MFC, on the anode and cathode sides, respectively. The inoculated bacteria are kept in the anaerobic environment with the substrate, and they need to attach to an electrode to give up the electrons from the substrate consumption because of the lack of oxygen as the direct electron acceptor. The electron charges in the anode create the potential difference between the cathode and the anode. Once the circuit is completed with a resistor, the electrons are transferred to cathode and reduce the oxygen from the air which is the terminal electron acceptor. Oxygen reacts with the hydrogen ions (protons) coming from the chemical reaction in the anode, which forms H_2O as a result at the cathode side. Besides, MFCs can also be used for hydrogen production, with a slightly change in the design.

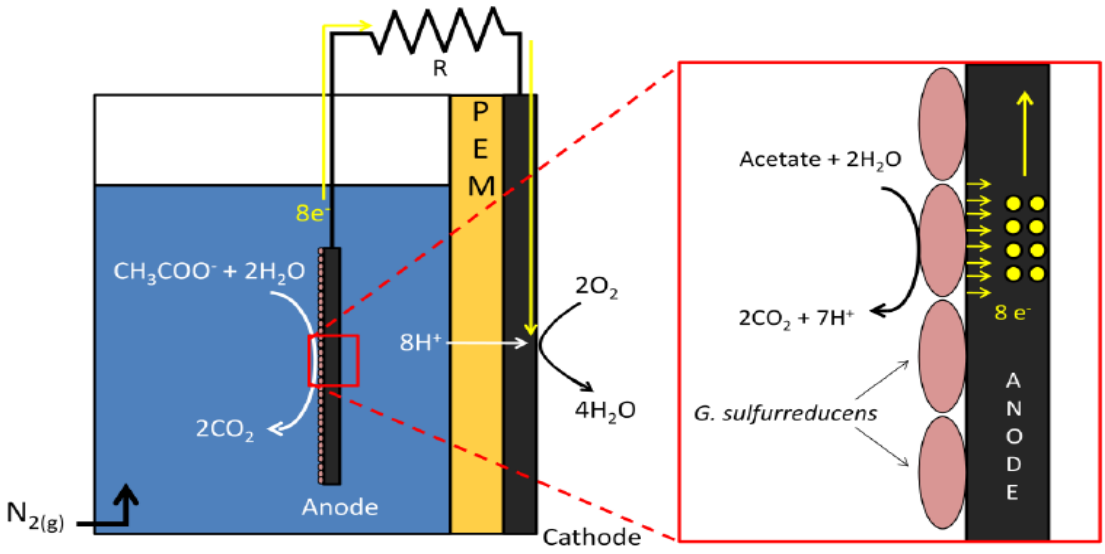

Figure 1.3 Typical schematic of single chamber air-cathode microbial fuel cell with PEM [9].

In Fig. 1.3, a representation of a typical single-chamber MFC with a PEM, with acetate as the substrate and *G. sulfurreducens* as the bacteria is shown. However, membrane-less MFCs are more widely used nowadays due to the high cost of PEMs [18].

In this study, a single-chamber air-cathode MFC is used with *G. sulfurreducens* as the bacteria and with acetate as the substrate.

1.2.2.2 Types of MFCs

MFCs can be distinguished by different characteristics, such as, their operation conditions, designs, the materials used, and the bacteria types [42], [21], [18], [25]. MFCs are mainly used in three modes: the continuous mode, the fed-batch mode, and the batch mode. In the continuous mode, the limiting substrates are constantly added to the reactor, while the output stream is simultaneously removed at the same rate, so as to keep the reactor volume constant. Design of control algorithms is significantly simpler for this mode than that for the fed-batch mode, since it is easier to stabilize the process at an equilibrium point. In the fed-batch mode the reactor is filled with a large amount of the limiting substrate and a small amount of the seed biomass. The system reaches a steady state and is harvested [28]. In both the continuous and fed-batch modes, MFCs act like other fuel cells, whereas if it is a batch system, an MFC would act like a bio-battery (in the sense of a battery which uses microorganisms to drive the chemical reactions). In the batch mode, unlike the fed-batch and continuous modes, the MFC can be perceived as a closed chemostat which does not have influx or discharging of substrate. The batch mode is used only for collecting the data in this study.

There are experimental studies on the continuous flow MFCs. In some studies [70], [40], the MFC performance is observed by changing the HRT (Hydraulic Retention Time). HRT gives a clue of how long it takes the substrate to be consumed in a reactor. It is usually expressed in hours and is mathematically described as the volume of the reactor divided by the influent flow rate. The dilution rate (which is preferred to be used in this study

instead of HRT), on the other hand, is the influent flow rate divided by the volume of the reactor. Du (*et al.*) observed that in the range between 10 and 100 mL/min, the flow rate is not the main factor significantly restraining the MFC performance [41]. The latter might be due to the inhibitors, such as pH being lower than the value 7 due to the hydrogen ions being accumulated in the anode, or the competition with other microorganisms which might dominate the flow rate effect. Nonetheless, flow rate change in a wider range could be effective on determining the MFC performance.

COD (chemical oxygen demand) is a measure of organic compounds in wastewater. It is an important parameter in MFCs if the purpose is wastewater treatment. In the continuous flow mode, the COD removal could be increased by increasing the HRT, but this would also reduce overall power and current generation due to lower average substrate concentrations [70]. These results demonstrate that the HRT will need to be selected on the basis of either optimizing energy production or COD removal [40].

MFCs can be operated with aqueous cathodes or air cathodes. The principle of MFC with an aqueous cathode is that water is bubbled with air to provide dissolved oxygen to electrode, whereas if it is an air cathode, one side of the cathode is exposed to the air which allows the oxygen to get through the cathode.

MFCs can also be classified by their designs, such as the single-chamber (usually membrane-less) configuration and the double-chamber configuration. A single-chamber MFC has both the anode and the cathode within the same space where the chemical reactions occur. A two-chamber MFC requires a membrane between the compartments to let the ions diffuse from one to the other.

1.2.2.3 Design Considerations

All the materials in an MFC system should be sterilizable (autoclavable) if only a certain type of microorganisms are desired in the MFC. The difficulty in achieving an optimal design comes from the considerations of a number of challenges, including choosing, autoclavable components, keeping the anode chamber anaerobic, and preventing the leakage, etc.

Practical applications of MFCs will require that we develop a design that will produce high power and Coulombic efficiencies. In addition, the economical aspect of commercialization (the manufacturing process being practical to implement on a large scale) and the studies on making affordable materials should be considered [18].

To address the low voltage of the MFCs, researchers focused on scaling up the MFCs, and for this purpose, single-chamber MFC is used due to its simplicity in scaling up. The study results demonstrate that the specific surface area of the cathode is the most critical factor for scaling up MFCs to obtain high power densities [23].

The spacing between the electrodes is highly affecting the power density. Two possible configurations are a separator electrode assembly or closely spaced electrodes that lack a separator, and the results suggest that separator electrode assembly designs can more effectively capture energy from wastewater, but closely spaced electrodes configurations will be superior in terms of treatment efficiency due to a greatly reduced time needed for treatment.

Reducing the distance between the electrodes using the separator electrode assembly design improved performance in terms of power production (0.328 Wm^{-2}) and energy recovery (25-78 Whm^{-3}) compared to the closely spaced electrodes design (0.282 Wm^{-2}, 2-34 Whm^{-3}) [22]. In a separator electrode assembly design, the electrodes are closely spaced but separated with a separator (to prevent short circuiting), whereas in a closely spaced elec-

trodes design, where a separator is absent, the electrodes are spaced 2 cm from the center point of the anode brushes to the cathode Pt/C catalyst surface [22].

1.2.2.4 Choice of Electrode Materials

The Coulombic efficiency, is defined as the ratio of total charges actually transferred to the anode from the substrate, to maximum possible charges if all substrate removal produced current [4]. A main challenge in constructing an MFC is to identify materials and the architecture that maximize power generation and Coulombic efficiency. Another challenge is to minimize cost and also to create design solutions that are inherently scalable (scaling up depending on the purpose of the use) [18]. Similar to other fuel cells, MFCs have two main electrode parts, an anode, a cathode, and in some cases, a separating membrane. The materials for these components are still a subject of active research. In particular, it is of interest to increase the efficiency and reduce the cost for the electrodes.

1.2.2.4.1 Anode materials: Electrode materials need to be investigated for good performance in MFCs. The electrode materials should have certain properties, such as high conductivity, high porosity, high catalytic activity with oxygen, being corrosion-resistant, high surface area, and being inexpensive. For the anode, the following materials are often used for/on anode materials due to their stability, high electric conductivity, and large surface area [18]:

- carbon paper, cloth, foams, and RVC (reticulated vitreous carbon);
- graphite rods, felts, foams, plates, and sheets;
- graphite granules;

- graphite fibers and brushes;
- conductive polymers;
- metals and metal coatings.

Among those, carbon cloth, carbon felt, graphite felt, carbon mesh and graphite fiber brushes are most commonly used in MFCs. The main reason why the graphite fiber brushes are frequently used is that they have the highest specific surface area and porosity [18].

1.2.2.4.2 Cathode materials: The cathode side is more complicated in terms of material science. The chemical reaction that occurs at the cathode is difficult to engineer as the electrons, protons and oxygen must all meet at a catalyst in a tri-phase reaction (solid catalyst, air, and water) [18].

The choice of the catalyst is crucial in the cathode material since it affects the diffusivity of oxygen in the MFC directly. Although platinum-coated electrodes are more efficient and superior than other electrodes in power production due to higher catalytic activity with oxygen, they are not cost-effective [19].

The materials often used for the cathode are [18]

- carbon cathodes with Pt catalysts;
- carbon cathodes with non-Pt catalysts;
- plain carbon cathodes;
- tubular carbon-coated cathodes;
- aqueous catholytes;

- Pt and Pt-coated metals;
- metals other than Pt;
- biocathodes.

Because the PTFE (polytetrafluoroethylene) diffusion layers coated on the air-cathode lets the oxygen get through easily, which does not require external air sparging to the cathode, air-cathodes with Pt catalyst are most commonly used in MFCs. Many researchers have chosen to use air-cathodes, as these types of electrodes will ultimately be the type of cathodes used in larger systems [18]. In this study, air-cathode wih Pt catalyst is used; however, some recent studies have focused on mesoporous nitrogen-rich carbon materials as cathode catalysts as an alternative to Pt catalyst [20].

1.2.2.5 Bacteria

MFCs started with the discovery of *E. Coli* bacteria producing electricity. M. Potter made the first attempt to produce electricity from this microorganism without a mediator (a chemical, such as neutral red, that transfers electrons from the bacteria in the MFC to the anode), where he used a platinum electrode [25]. However, since *E. Coli* could not transfer its electrons without a mediator, this study did not catch much interest. In 1980s, it was discovered that the current density and power output could be greatly enhanced by the addition of electron mediators [42].

Recent studies show that there are a wider range of bacteria options to use in MFCs, and there is no need for mediators since most of the bacteria can use special methods to give their electrons to the electron acceptor (anode). These bacteria that can transfer the electrons outside of their cells are called *exoelectrogens* [18]. Most frequently used bacteria

for MFCs with this property are Shewanella, Rhodoferax and Geobacter strains.

1.2.2.5.1 Important factors that affect bacterial growth: Chemical reactions are influenced by the temperature, so bacterial growth is also affected by the temperature change in the environment. For each type of bacteria, the growth rate increases with the temperature, and, in general, the rate doubles [1]. Even though temperature is not a big issue for MFCs in general, temperatures above the normal range for the species can destroy the enzymes and the organism may die.

The pH also affects the growth and most species of bacteria have a narrow pH range for growth, and for most organisms this range lies between 6 and 8 [1]. The study also suggests that, the design and operation of an MFC-based treatment system must consider the optimum pH conditions required for growth of the bacteria of interest.

If the bacteria require an anaerobic environment (for example, Geobacters), the presence of molecular oxygen would affect the growth ability of bacteria significantly. For the terminal electron acceptor, some bacteria can use nitrite or sulfate instead of oxygen. But since oxygen is easily found in the air and the reduction of oxygen would have more Gibbs free energy, it is generally preferred to use oxygen as the electron acceptor in MFCs.

Microbes transfer electrons to the electrode through an electron transport system that either consists of a series of components in the bacterial extracellular matrix or together with electron shuttles dissolved in the bulk solution [42]. Most studies thus far have focused on investigating the electron transfer mechanisms that enable Geobacter biofilms to reduce the electrode [10].

1.2.2.5.2 Energy capture mechanism in bacteria: The electron carriers can be divided into two different classes, those that are freely diffusible throughout the cell's cyto-

plasm and those that are attached to enzymes in the cytoplasmic membrane [1]. There are co-enzymes in the bacteria which carry the useful energy. The co-enzyme $NADP^+$ is involved in anabolic reactions while NAD^+ in catabolic reactions. The particular electron carriers that operate in a given cell depend upon the relative energy levels of the primary electron donor and the terminal electron acceptor [1].

NAD^+ extracts two protons and two electrons from a molecule being oxidized and in turn is converted to its reduced form, $NADH$. The reactions of NAD^+ is,

$$NAD^+ + 2H^+ + 2e^- = NADH + H^+ \tag{1.1}$$

The Gibbs free energy for this reaction is

$$\Delta G = 62 \quad \text{kJ} \tag{1.2}$$

Similarly, $NADP^+$ takes two protons and two electrons from the substrate and form $NADPH$:

$$NADP^+ + 2H^+ + 2e^- = NADPH + H^+ \qquad \text{where} \qquad \Delta G = 62 \quad \text{kJ} \tag{1.3}$$

When the Gibbs free energy is positive, it means that energy must be taken from the organic molecule in order for $NADH$ to be formed. When the $NADH$ in turn gives up the electrons to another carrier and is reduced back to NAD^+ (Fig. 1.4), it also gives up the chemical energy, which may be converted to other useful forms [1] and form the first part of ETC (electron transport chain).

In natural environments oxygen is the terminal electron acceptor for the bacteria, and the energy released as the electrons are passed through a chain of electron carriers (Fig. 1.4)

to oxygen can be determined from the overall Gibbs free energy change of the $NADH$ and O_2 half reactions,

$$NADH + H^+ = NAD^+ + 2H^+ + 2e^- \qquad \Delta G = -62 \quad \text{kJ} \tag{1.4}$$

$$\frac{1}{2}O_2 + 2H^+ + 2e^- = H_2O \qquad \Delta G = -157 \quad \text{kJ} \tag{1.5}$$

Net reaction is:

$$NADH + \frac{1}{2}O_2 + 2H^+ = NAD^+ + H_2O \qquad \Delta G = -219 \quad \text{kJ} \tag{1.6}$$

Therefore, the energy transferred along with electrons from an organic chemical to $NADH$ is released to subsequent electron carriers and ultimately to oxygen in aerobic respiration. However, in MFCs a portion of this energy is going to be captured by the anode before by oxygen. This energy transfer results in -219 kJ per mole of $NADH$ for use by the organism in the aerobic case. The bacteria is using a portion of this energy for maintenance, cell synthesis, growth, etc. The primary example of an energy carrier for this purpose is adenosine triphosphate (ATP) (Fig. 1.4). When energy is released from an electron carrier, it is used to add a phosphate group to adenosine diphosphate (ADP) [1],

$$ADP + H_3PO_4 = ATP + H_2O \qquad \Delta G = 32 \quad \text{kJ} \tag{1.7}$$

Geobacter belongs to dissimilatory metal reducing microorganisms, which produce biologically useful energy in the form of ATP during the dissimilatory reduction of metal oxides under anaerobic conditions in soils and sediments [42].

Therefore, NAD^+ captures protons and forms $NADH^+$. Then $NADH$ diffuses through bacteria cytoplasm and forms NAD^+ and one proton by releasing electrons (energy). Some of this energy is used by bacteria to form ATP which they need for cell synthesis and for cell maintenance. Whenever bacteria needs energy, it reduces ATP to ADP and this ADP later takes the same cycle to form ATP from $NADH$ to NAD^+ reaction.

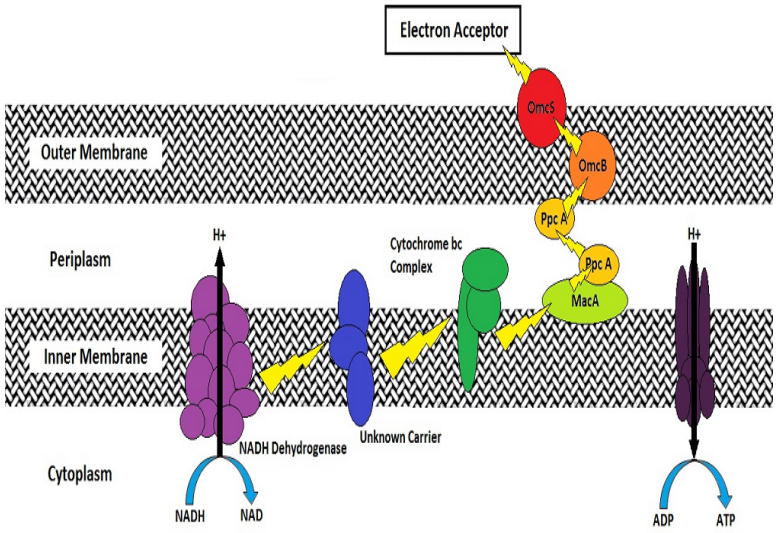

Figure 1.4 Schematic of the electron transport chain (ETC) through the bacteria to the electron acceptor [26].

1.2.2.5.3 Electron transfer mechanism: After bacteria capture the energy from the substrate, they give out the electrons to an electron acceptor which is the anode in MFCs. It is still not fully understood how bacteria transfer their electrons outside of their outer membranes. However, there is an agreement on three different types of extracellular electron transfer (EET), by different microorganisms. In Fig. 1.5, the three discovered EET are depicted.

The first mechanism is explained as that bacterial electron carriers through the ETC give the electrons through the outer membrane to a solid electron acceptor. Bacteria using this

mechanism require direct contact with the solid electron acceptor and, thus, cannot form a biofilm [37]. The second mechanism needs a mediator, which helps carry the electrons from the bacterial outer membrane to the solid electron acceptor.

The third proposed mechanism involves a solid component that is part of the extracellular biofilm matrix and is conductive for electron transfer from the bacteria to the solid surface [37]. This mechanism is supported by the recent discovery of the possible role of cellular pili as nanowires (which some bacteria, such as *G. sulfurreducens*, produce to attach the electrode) [17], which are being characterized for their capability to conduct electrons [37].

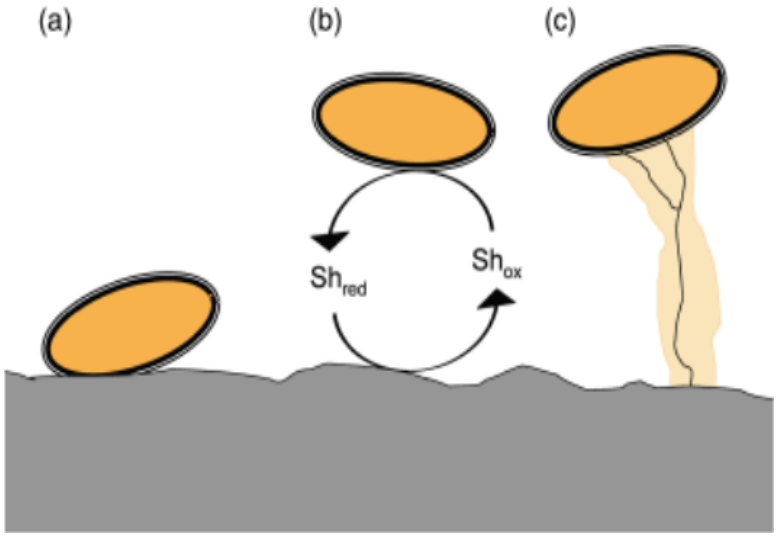

Figure 1.5 Schematic of three EET (extracellular electron transfer) mechanisms used by ARB (Anode-respiring bacteria) (that is how Cesar I. Torres define the bacteria in MFC): a) direct electron transfer, b) an electron shuttle, and c) a solid conductive matrix [37].

1.2.2.6 Substrate

Substrate is considered to be a key factor for MFCs since it has the source for the organic matter which bacteria use to extract energy. There are a large number of substrate types used in MFCs.

It is difficult to compare the performance of MFCs from the literature by the substrate used, due to the different operational conditions in each study. There are some measures, such as current density, that can help us understand the effect of substrates. The unit used for current density is usually (mA/cm^2). The majority of MFC researchers use acetate as the substrate since it show the highest energy output from MFCs comparing to other single substrate types [21].

There are studies that point to the importance of the substrate on the power density and present relevant mathematical models [1], [18], [35], [37]. For example, it is shown [23] that the substrate concentration has a significant effect on the potential on the anode side but not cathode performance, while the solution conductivity has a significant effect on the cathode but not the anode performance.

1.2.3 MFC Modeling

In this section, for the purpose of modeling and controlling MFC, the relevant literature is critically reviewed. To derive a mathematical model for an MFC, one should start with understanding the bacteria characteristics, microbial kinetics, and anaerobic digestion. There are vast amount of literature about the microbial kinetics which explains the microorganism behavior in details [1], [13], [14], [15].

1.2.3.1 Anaerobic Digestion

Anaerobic digestion is a process where organic matter is degraded into a mixture of methane, carbon dioxide, and biomass [51]. Among the diverse process designs and configurations for anaerobic treatment processes (e.g., anaerobic suspended growth, up-flow and down-flow anaerobic attached growth, anaerobic lagoons, up-flow anaerobic sludge blanket), some pre-

viously developed anaerobic digestion models can give important information about kinetics of reaction, transport, and space limitations for the MFC anode [39]. The anaerobic digestion models considered in this study involve anaerobic suspended growth and the biofilm attachment.

1.2.3.2 Microbial Kinetics

There are two common descriptions for the substrate consumption kinetics and the microorganism growth rate, Monod kinetics and the Haldane kinetics. Monod kinetics was named after microbiologist Jacques Monod, in 1940s, and is also called Michaelis-Menten kinetics [11]. In the literature, Haldane kinetics usually is used for the optimal control purpose for the anaerobic digestion, such as that in [59]. One of the reasons that Haldane kinetics is used in nonlinear analysis is because it considers the inhibitors. And with that difference from the Monod kinetics, an interesting phenomena, the singular arc, occurs in the optimal control analysis [67]. However, in this study Monod kinetics is considered due to its better accuracy to represent MFC models. The Monod equation,

$$\mu = \mu_{max} \frac{S}{K + S} \tag{1.8}$$

expresses that, at a high substrate concentration, the process is at its maximum rate, while at a low substrate concentration the substrate becomes rate limiting for the system. Here, $\mu_{\max}$ is the maximum specific growth rate, S is the concentration of rate-limiting substrate, and K is the concentration giving one-half the maximum rate. Eq. (1.8) represents the microbial kinetics for one substrate. It can also be modified if there are more than one

substrate in the media [35]; for example, for two substrates S_1 and S_2,

$$\mu = \mu_{max} \frac{S_1}{K_1 + S_1} \frac{S_2}{K_2 + S_2} \tag{1.9}$$

Over the years, many different anaerobic digestion models were studied [51], [56], but their uses were limited to specific applications [39]. Due to the different approaches, IWA (Internaional Water Association) developed a generalized anaerobic digestion model, ADM1 (Anaerobic digestion model no 1) [58]. The ADM1 model processes included many details, such as, acidogenesis from sugars, acidogenesis from amino acids, acetogenesis from long chain fatty acids, acetogenesis from propionate, acetogenesis from butyrate and valerate, aceticltastic methanogenesis and hydrogenotrphic methanogenesis [58]. The complexity of this model requires large computational effort and creates challenges in model parameter identification, which means that parameter estimation algorithms could not fit such a large number of parameters within reasonable confidence levels [53]. For that reason, ADM1 is not taken as the base model for this study.

1.2.3.3 Biofilm Modeling

ADM1 did not consider the biofilm growth; instead it assumed a well-mixed chemostat for the anaerobic digestion. In the MFCs bacteria usually form a biofilm on the anode surface, which becomes a solid conductive layer in the sense of electron accepting. In [52], the authors used several microbial species and observed the competition for space and substrate. They used the continuum approach, mass balance equations, and experimental observations to describe the effect of relative substrate concentrations on biofilm performance and composition [52].

The modeling of biofilm formation in MFCs can be highly complex. In the study [48], the

authors modeled a mixed population biofilm formation in three dimensions. The diffusion of several substrates and the growth of different microorganisms were modeled using PDEs (partial differential equations) due to the nature of the biofilm modeling. In the paper [35], the authors developed a dynamic, one-dimensional, multi-species model for the biofilm in the anode of an MFC. They concluded that the biofilm conductivity strongly influences the electron donor, current fluxes, and the biomass distribution. They used the anode potential to derive the model. In [37], the authors aimed to evaluate how well each extracellular electron transfer (EET) mechanism can produce a high current density without a large anode potential loss by using the biofilm model. The complexity of these models is similar to that of ADM1, which requires large computational effort.

1.2.3.4 MFC Model Comparisons

Some MFC models are too complex to solve and some of them are not well suited for control. Table **??** summarizes the characteristics of available MFC models in terms of anode or/and cathode types, microorganisms, biofilm existence, and the convergence difficulty (whether the models would demand large computational effort to be solved).

In MFC research with the wastewater as the substrate, multi-species are often considered. In this study, pure culture (single-microorganism) is considered and the necessity of fast convergence is taken into account in the model analysis.

1.2.3.5 Anaerobic Digestion Model Analysis

Modeling of anaerobic digestion and two main kinetics (substrate utilization and the microbial growth rate) has been well studied [2], [57]. These models have been investigated for their system properties in a few cases, including stability analysis of the equilibria, feedback

Table 1.1 Comparison of characteristics included in all available MFC models [39].

Model	Type of MFC model	Multi-species	Biofilm	Ease of convergence
$ZhangandHalme(1995)$	$Anodeandcathode$	No	No	Yes
$Zengetal.(2010)$	$Anodeandcathode$	No	No	Yes
$Macusetal.(2007)$	$Onlyanode$	$No*$	Yes	Yes
$Hamelersetal.(2011)$	$Onlyanode$	No	Yes	Yes
$Picioreanuetal.(2007)$	$Anodeandcathode$	Yes	Yes	No
$Picioreanuetal.(2010a)$	$Anodeandcathode$	No	No	No

*This model assumed inert and active biomass competing only for space on the anode surface.

stabilization, robust stabilization with Lyapunov method, and optimal control of the system.

A stabilizing feedback control was designed for Haldane-Monod model of bacterial growth [66]. More recently, the authors of [68], studied optimal control of a nonlinear fed-batch bioprocess using a predictive approach. Stability analysis, nonlinear analysis, and control of anaerobic digestion were performed using similar model kinetics [31], [43]. For the stability analysis of the chemostats appropriate Lyapunov functions were chosen by some researchers [63], [28]. On the control side, there have been studies focusing on feedback design [30] for different purposes, such as to regulate the organic pollution level [61] using the similar anaerobic digestion model. There are also studies on nonlinear adaptive control for bioreactors [62] in which the authors proposed a nonlinear controller and proved the global asymptotic stability of the closed-loop system.

Despite the aforementioned progresses, the works cited above mostly deal with bioreactors, not for MFCs. Even though an MFC includes biofilms, its unique characteristics offer new opportunities for modeling, analysis, and control design.

1.2.4 Control of MFCs

There are numerous studies on the control of fuel cells since they have complex systems with numerous equipment components, such as pumps, compressors, storage tanks, flow meters, and sensors. On the other hand, for the control of MFCs, due to its relatively new nature, research effort has been very limited.

Theory and experiments with the nutrient flow control for maximizing the amount of microorganisms were explored by the authors of [66]. In this study, a stabilizing feedback control was designed for Haldane-Monod model of microbial growth of *E. Coli*. In another study [61], a control law was proposed to drive the model to a desired set point for any initial operating conditions for an anaerobic digestion. The authors concluded that COD (chemical oxygen demand) of wastewater can be estimated on-line without the need for sensors. The latter work was only focused on a chemostat which had an anaerobic digestion, and thus is different from an MFC..

Researchers have conducted studies on parameter estimation for the MFCs [39]. In this study, the authors considered multi-species for microorganisms and wastewater as the substrate for the anaerobic digestion. They modeled MFC based on the mixed system (not biofilm) assumption, explored the effect of the external resistance on the performance, and optimized the substrate consumption by staging MFCs. They also concluded with R_{int} and E_{OCP} estimations as follows,

$$R_{int} = R_{MIN} + (R_{MAX} - R_{MIN})exp^{-K_R X} \tag{1.10}$$

$$E_{OCP} = E_{MIN} + (E_{MAX} - E_{MIN})exp^{(\frac{-1}{K_R X})} \tag{1.11}$$

R_{MIN} is the lowest observed internal resistance and R_{MAX} is the highest observed internal resistance. E_{MIN} is the lowest observed OCP and E_{MAX} is the highest observed OCP. K_R is the constant which determines the curve steepness and it can be obtained using the voltage measurements from the operated MFC. The R_{MIN}, R_{MAX}, E_{MIN} and E_{MAX} values were obtained from the polarization tests. In the same study, they used mediators, but in most of MFC studies mediator-less bacteria are used due to the extra expense of mediators [40], [41], [45], [18], [10], [46].

There have been some attempts on maximizing the power output with power management systems and PID controllers [45], [38] for MFCs, but there has been little experimental work in these studies to support the simulation results.

1.3 Conclusion

In this chapter, an introduction to MFCs is carried out with the background and an extensive literature review on the modeling and control issues. It has been concluded that there is not adequate work on control of MFCs, even though it is an important area which is directly related to the MFC performance, cost reduction, and better understanding of the system. It has been realized that there are different models describing microbial kinetics, and in this study Monod kinetics is selected, since it does not include the inhibitor effect and is a better representation for MFC systems. For the model analysis, there has been research on anaerobic digestion and microbial kinetics model analysis for bioreactors. However, such analysis has not been applied to MFC models with the specific parameters for MFC dynamics.

1.4 Objectives

The goal of this research is to understand the mathematics, theory, and mechanism behind the MFC systems with the available models, and to further investigate the dynamic model in order to develop an MFC control system for its performance optimization.

Therefore, the objectives of this study are

1. To design an MFC which can serve in batch, fed-batch and continuous modes and be used as a platform for collecting experimental data.

2. To find a model for electricity generation from MFCs that can be validated with experiments. Substrate and microorganism concentrations are to be used as the state variables in the model.

3. To analyze the system based on nonlinear systems theory, including the stability of the equilibrium points.

Chapter 2

Design and Development of an MFC

In this chapter, the design and prototyping of an MFC are presented. This MFC is subsequently used in model development and analysis. The experiment setup used in SML is shown in Fig. 2.1. A potentiostat is used to collect the data and send it to the dSpace ControlDesk. D-Space uses Matlab/Simulink in its interface. The system (both MFC and the storage containers) were bubbled with nitrogen constantly, from the nitrogen cylinder. There are autoclaved syringe needles on the top of both MFC and storage containers to let the oxygen bubbled out. Filters are used to keep the nitrogen gas sterile. To show the pH buffer effect, samples were collected from the MFC on a regular basis. Samples were taken with the aid of a sterile syringe and samples are also used for the HPLC analysis in Reguera lab at MSU.

2.1 MFC Design and Fabrication

2.1.1 Anode

The anode material used in the MFC in this study was carbon fiber (PANEX 35 50K, Zoltek) brush with two twisted Ti (Titanium) wires. The specifications for the brush (The Mill Rose Company, Mentor, OH, USA) are 1.989 inches in diameter (Fig. 2.2), 2.75 inches in length for the brush part, and 4 inches in overall length with the Ti part included. Carbon fiber

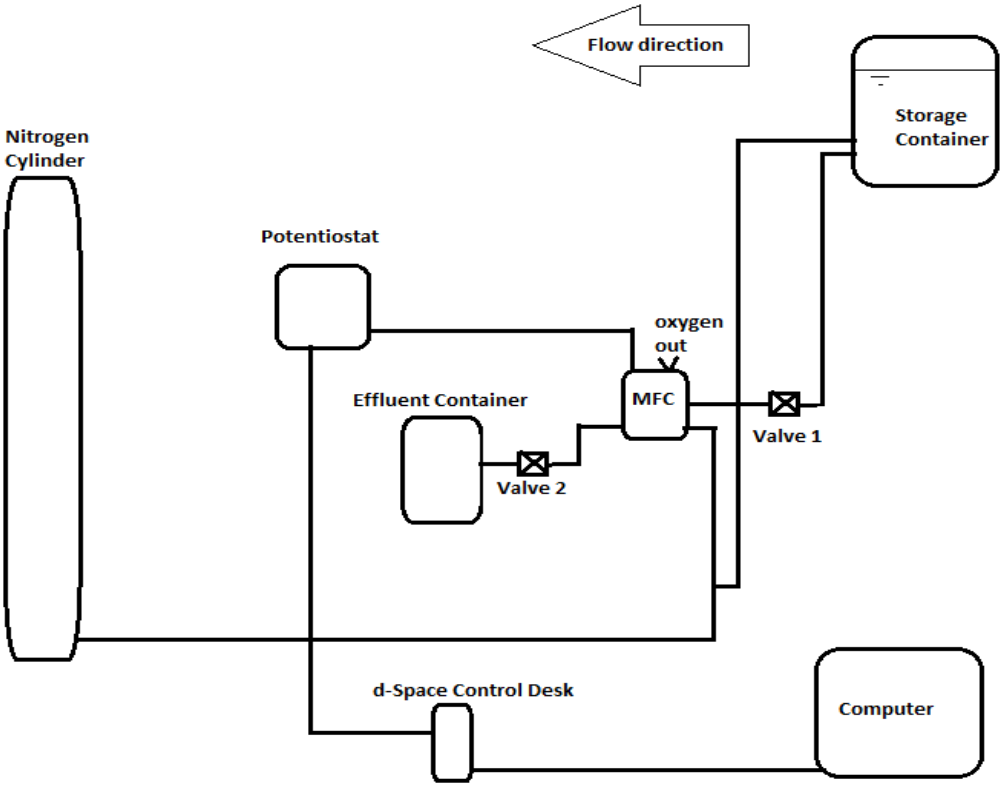

Figure 2.1 The MFC experimental setup used in this study.

brushes were soaked in the acetone overnight and then heat-treated at 450°C for 30 min [33] in the Physics Laboratory at MSU.

Figure 2.2 Anode brush that was prepared in SML-MSU.

The reason why a brush-type electrode was chosen was that it has higher surface area than other carbon felt anodes. In the experiments, only some portion of the anode brush was in contact with the medium because of the short length of the Ti wire on the anode brush (Fig. 2.6). The active anode brush surface area was calculated to be approximately 0.67 m^2.

2.1.2 Cathode

The cathode was manufactured in different laboratories at MSU. The cathodes were made by applying platinum and four diffusion layers on a teflon-treated carbon cloth as described in [24]. The materials used for this process and detailed information are shown in Table 2.2.

First, the carbon base layer was prepared using the carbon cloth, carbon black powder, and 40% PTFE solution. This 40% PTFE solution was prepared from 60% PTFE solution (Table 2.2), by dilution with DI (deionized water). The whole mixture was kept in the plastic sample vial tube. Solid glass beads were added into the tube to help forming homogeneous mixture. The mixture was mixed with a vortexer (Vortex-Genie mixer, S8223, Scientific

Table 2.1 Materials used for the cathode fabrication and their specifications.

Material	**Vendor**	**Address**	**Specification**
Carbon cloth	ElectroChem Inc.	MA, USA	Teflon-treated, dimensions 19cm x 19cm
PTFE (Polytetrafluoroethylene)	Sigma-Aldrich	USA	60 wt % dispersion in H_2O
10% Pt/C catalyst	ElectroChem Inc.	MA, USA	Weight 10wt% platinum, Vulcan XC-72 carbon, amount 5 grams
Nafion perfluorinated resin solution	Sigma-Aldrich	USA	5 wt. % in mixture of lower aliphatic alcohols and water, contains 45% water
Carbon black powder	Cabot Corp.	GA, USA	Vulcan XC72 Conductive Carbon Black
Propanol	Alfa Aesar	MA, USA	2-Propanol, Spectrophoto-metric Grade, 99.7+%
Solid Glass Beads	Propper Manufacturing Co. Inc.	NY, USA	3mm in diameter

Industries, Inc., USA) in the Robotics and Automation Lab at MSU. Then this mixture was coated on the carbon cloth with a small, soft paintbrush. The carbon cloth with the coating was heat-treated on a heat-resistant glass ceramic plate (McMaster Carr) in a furnace (Physics Laboratory at MSU) at 370°C for 25 min. Secondly, 60% PTFE solution was applied on the previously coated side to form the diffusion layer. The optimum layer number was found to be four according to [24]. The carbon cloth with the PTFE coating was heat-treated on the same furnace at 370°C for 12 min between each layer. Finally, the catalyst layer was applied. The materials used for this stage were 10% Pt/C, nafion, propanol, and DI (Table 2.2). More detailed information about this whole process can be found in [44].

The Pt/C catalyst side of the air-cathode is in contact with the media in MFC whereas the PTFE layer helps the oxygen get through to form the H_2O (Fig. 2.3).

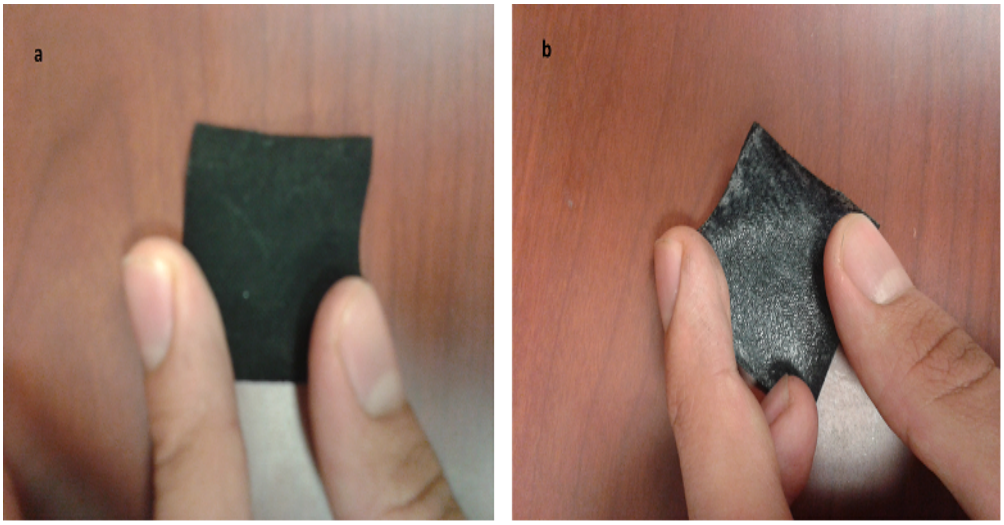

Figure 2.3 Cathode material that was fabricated in SML-MSU. a) The Pt/C catalyst side. b) The PTFE diffusion side.

2.1.3 The First Prototype

In this study, a single-chamber rectangular prism-shaped air-cathode MFC (Fig. 2.4) was first built in SML. To prototype this design, round, impact-resistant polycarbonate tube and sheets (McMaster Carr) were used. The total liquid volume was 230 ml.

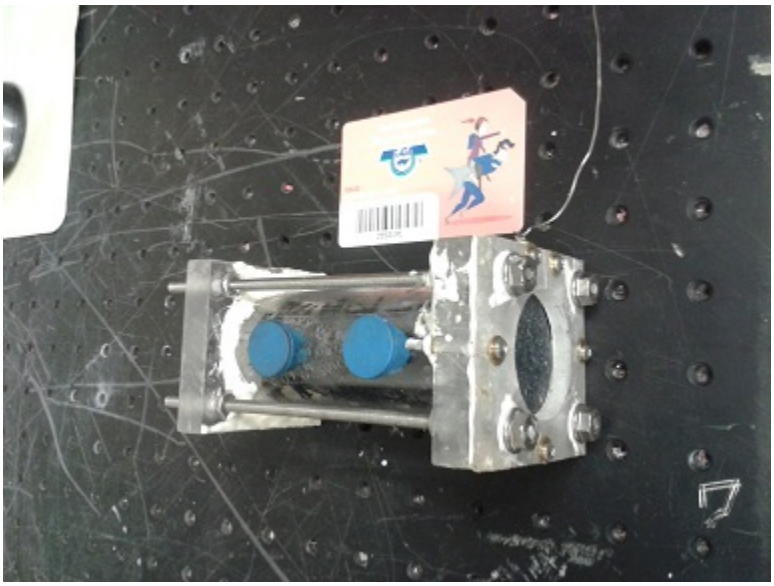

Figure 2.4 A single-chamber air-cathode MFC that was built in the Smart Microsystems Lab.

The system would be operated in a batch mode and with different substrate concentrations; however, the cathode section of the MFC had too much leakage for its total liquid volume. The leakage problem could not be resolved with a few different attempts, because of the difficulty associated with the choice of autoclavable materials and because of the anaerobic requirement. For that reason, an alternative bottle-shaped design was considered, as discussed next.

2.1.4 The Second Prototype

In this new design, there was still leakage on the cathode part; however, it could be solved by sealing the cathode extension with waterproof autoclavable silicon (ACE Hardware, MI, USA). The leaking problem was from the external pressure, which came from the nitrogen cylinder for keeping the system anaerobic. In the current design (Fig. 2.7) the spacing between the anode brush and the cathode was 2 inches. This MFC system can be used for batch, fed-batch, and continuous systems.

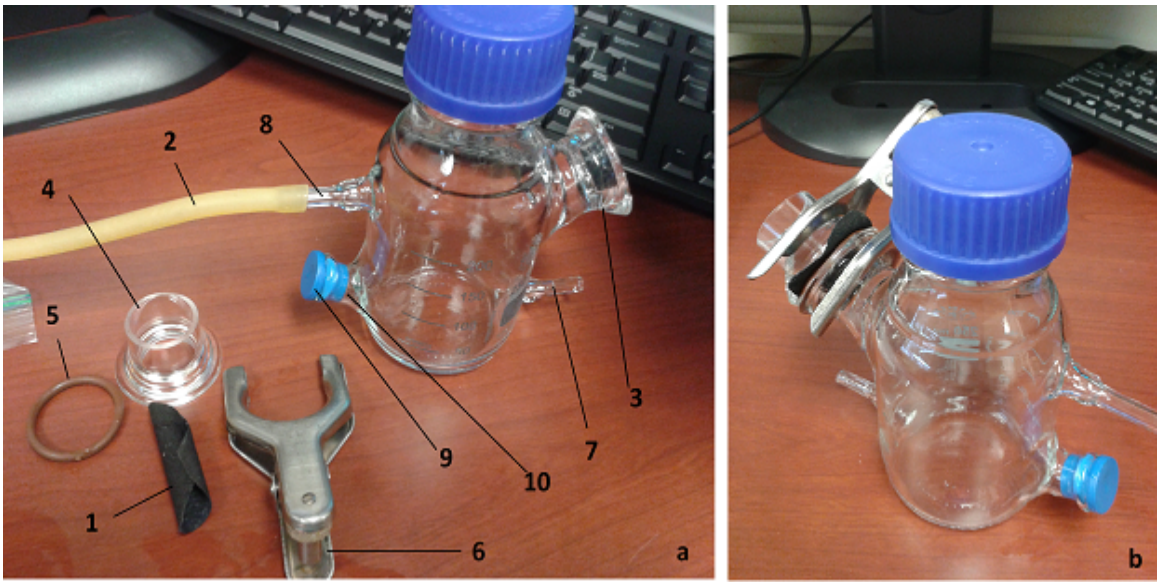

Figure 2.5 a) The components of the MFC compartment for continuous or fed-batch system. b) The assembled view of the components.

The components shown in Fig. 2.5 include, 1) cathode that was fabricated, 2) autoclavable tubing for the substrate flow, 3) the arm extension for the cathode placement, 4) a glass part which sandwiches the cathode, 5) o-ring, 6) clips to hold the cathode between the glass and the extension arm, 7) inflow extension barbed fitting, 8) outflow extension barbed fitting, 9) blue butyl stopper, and 10) the extension for the reference electrode and for the N_2 inflow.

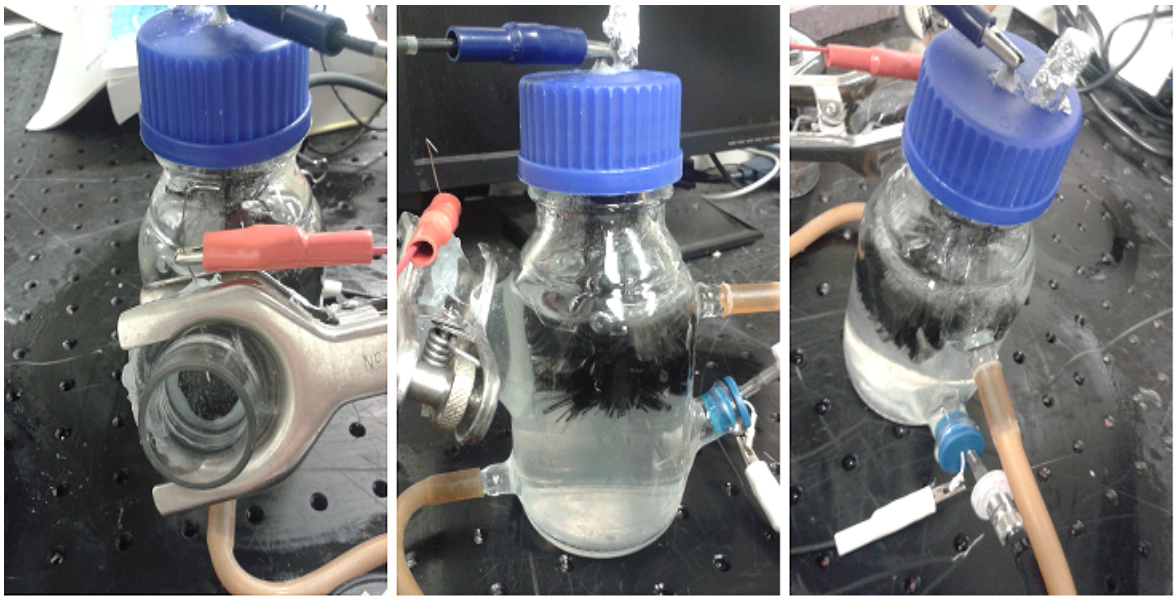

Figure 2.6 The assembled MFC prototype with the anode, cathode and acetate as the substrate.

2.1.5 Other System Components

The MFC system was designed to be used for both the batch mode and the fed-batch mode (even though it can be used also for the continuous mode), and it requires the ability to modulate the medium flow. Two solenoid valves were used with one normally opened (NO) (Honeywell, model no: 71225SN2EF00N0C111B6, MI, USA) and the other normally closed (NC) (Parker, model no: 71215SN2MF00N0C111P3, MI, USA). The specifications for the valves were, 120/60 volts/Hz, 10 Watts,, 750 psi. The valves 1/4 inches with a 3/64 inches orifice size ($C_v = .005$). The NC valve was used for outflow while the NO valve was used for inflow to the MFC.

For data acquisition and system control, dSpace Control Desk 5.1 was used with a computer. DSpace required $-10/+10$ volt as an input/output, so SSRs (Solid State Relays) (Opto22, CA, USA) were used, along with the fuse, to convert the digital signal (VDC) to 120 VAC to operate the solenoid valves.

Autoclavable glass media/storage bottles (United States Plastic Corp., OH, USA) used to store the media and to operate the MFC. The glasses were re-shaped (Glasswork at the Chemistry Building, MSU) based on the purpose of this study. The bottle where the MFC was operated was 250 ml, the one which stored the input medium was 1000 ml and the effluent storage bottle was 500 ml.

The system needs to be kept anaerobic. Therefore, a nitrogen cylinder with 99.999% purity, 304 SCF (standard cubic foot) (MSU Stores) kept pumping the nitrogen into the MFC bottle to get oxygen out of the system. To lower the high pressure of the nitrogen cylinder, a regulator (SMITH Equipment, SD, USA) was used so that the outlet pressure was always less than 5 psi. Specifically, both the MFC bottle and the input storage bottle needed to be kept anaerobic so the nitrogen gas was splitted to the bottles with a splitter. Tubing used for this purpose was masterflex norprene tubing (Cole-Parmer Instrument Company, IL, USA). Sterile needles and luer locks were used to get through the blue butyl stoppers (Fisher Scientific Company, PA, USA) to the MFC. A needle was attached to the top of each bottle to release the oxygen. PTFE syringe filters (Fisher Scientific Company) were attached to the needles to keep the nitrogen gas sterile. Autoclavable tubing (McMaster Carr) with brass-barbed fittings were used to let the substrate flow in the system.

An Ag/AgCl reference electrode with flexible wire connectors (BASi, IN, USA) was used for the anode electrode potential measurement. An external Ti wire, 0.5 mm in diameter, was used on the cathode side for the closed-circuit data acquisition.

There were other materials and safety equipment used for the fabrication and operation, such as 50 mL conical polypropylene centrifuge tubes for mixing the solutions and preparing the pH buffers, distilled water for the pH calibration, acetone for the anode brush treatment, glasses, face shield, nitrile purple gloves and goggles for safety (MSU stores). All components

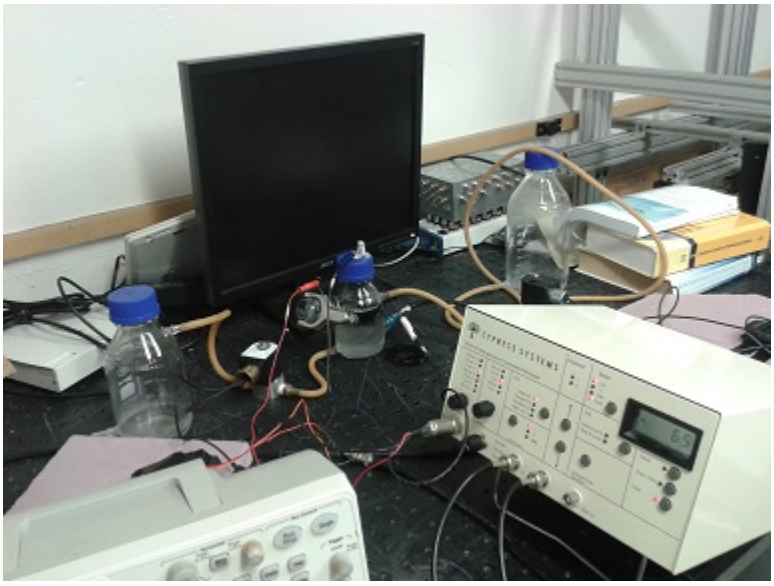

Figure 2.7 Experimental setup for MFC characterization and model development.

of the MFC system were autoclaved for 30 min under 24 psi pressure value with 121°C with gravity cycle (steam displaces air in the chamber by gravity, i.e. without mechanical assistance, through a drain port) at the same time in an oven at the Reguera lab at MSU.

2.1.5.1 pH Buffer Preparation and Calibration

The pH probe needed to be calibrated each time before it was used. For the calibration, three different pH buffer solutions (of pH 4, 7 and 10) were prepared. Buffer capsules (order code PHB) were used for preparing the pH buffer solutions. Powder from each capsule was added into 100 mL of distilled water in a plastic bottle. Then 3 drops of buffer preservative (Micro Essential Laboratory, Broklyn, NY, USA) were added to prevent mold growth and to add color to the solution so each solution can be identified.

- Blue pH 10 (with tolerance of 0.02) at 25°C
- Green pH 7 (with tolerance of 0.02) at 25°C
- Orange pH 4 (with tolerance of 0.02) at 25°C

After the buffers were prepared, the pH probe was used to have three different value points. These three points were used to have the following equation. For the pH measurement, samples were taken with a syringe (slip tip 20 mL, MSU Stores) from the MFC container.

$$pH \quad value = -2143 * (Voltage \quad value) - 33.2884 \tag{2.1}$$

2.2 Inoculum and Medium Composition

2.2.1 Bacteria

G. sulfurreducens strain PCA was used for this study. It was inoculated for the control purpose with the fed-batch mode in our experiment and was routinely cultured anaerobically in the DBAF (DB with fumarate and acetate) medium, which was DB medium [3] supplemented with 20 mM acetate as the electron donor and 40 mM fumarate as the electron acceptor.

Na_2SeO_4 (1 mM) was also added to stimulate growth, as reported elsewhere [3]. The MFC was inoculated with cell suspensions as described previously [3], except that the electron donor in the anode chamber was acetate, which had an initial concentration of 3 mM for first experiments, and for the latter experiments, the acetate medium had an initial concentration of 1 mM.

The bottles for bacteria were top out at optical density at OD_{600} (optical density at 600 nanometer) of 0.6, and 100 mL of this culture was spun down, washed twice and then resuspended in 10 mL of medium for the inoculation to the MFC. The initial cell concentration was calculated to be approximately $5x10^{10}$ cells/mL.

Table 2.2 The ingredients and amount added for 3 mM acetate in 1300 mL total volume of medium.

Ingredients	**Amount added**	**Units**	**Final concentration**
10X DB Stock	130	mL	
100X DB Mineral Mix	13	mL	
100X DL Vitamin Mix	13	mL	
0.75 M NaAcetate	5.2	mL	3
KH_2PO_4	2.054	g	116 mM
K_2HPO_4	1.9032	g	84 mM
Double distilled H_2O Fill To:	1300	mL	

Table 2.3 The ingredients and amount added for 1 mM acetate in 2000 mL total volume of medium.

Ingredients	**Amount added**	**Units**	**Final concentration**
10X DB Stock	200	mL	
100X DB Mineral Mix	20	mL	
100X DL Vitamin Mix	20	mL	
0.75 M NaAcetate	2.67	mL	1
KH_2PO_4	31.6	g	116 mM
K_2HPO_4	29.28	g	84 mM
Double distilled H_2O Fill To:	2000	mL	

2.2.2 Substrate

In the first experiment, 3 mM acetate concentration was used. The substrate was prepared (see Table 2.3) at the Reguera lab at MSU. In latter experiments, 1 mM acetate concentration was used (Table 2.4).

After the acetate and other ingredients with the pH buffer were mixed in 2000 mL total volume, pH was recorded as 6.46. Then NaOH was added to set the pH at 6.73. Then the medium was transferred to the side-arm flask and vacuumed with rapid stirring for 30 min. After the vacuuming, it was splitted into 200 mL bottles with pressure tubes and sparged with N_2:CO_2 (80:20) first without stoppers for 30 min and then with stoppers for another 30 min. The bottles were crimped and autoclaved at 121°C for 30 min in the dry mode.

2.3 Data Acquisition

Data were collected from a potentiostat (Omni-101 Potentiostat, Cypress Systems). Potentiostats are devices which control potential to give the information about the characteristics of the electrochemical device (MFC in this case). A potentiostat works with three electrodes, the working electrode (the anode), the Ag/AgCl reference electrode, which has a fixed potential, and the auxiliary (counter) electrode (the cathode). To measure the open circuit potential of the anode, the rotary controller on the potentiostat should be on standby. To fix the anode potential at a certain value, the potentiostat rotary controller was switched to cell-on and the value of the anode potential was set at +0.240 V. That way, the bacteria would be driven to attach to the anode and form a biofilm. Everything was measured and displayed with dSpace (Control Desk 5.1 with CP1104 board). The current was measured through a circuit because dSpace (Fig. 2.10) accepted only voltage inputs.

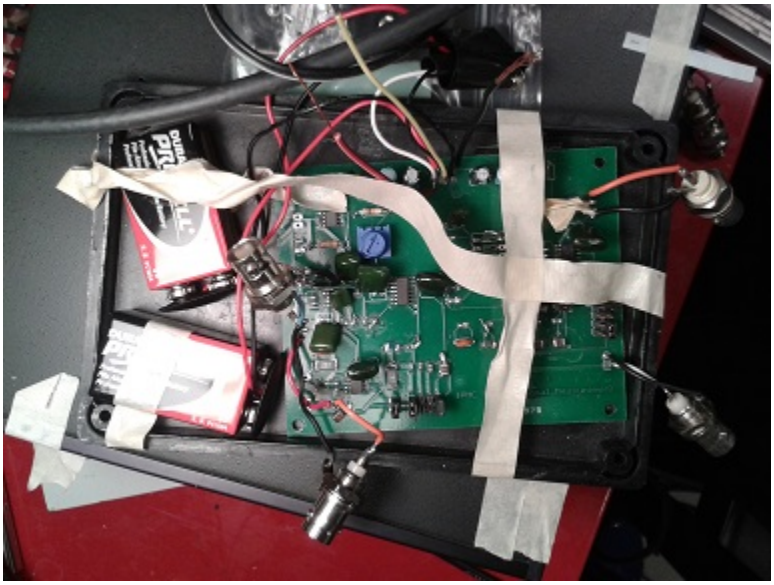

Figure 2.8 The circuit used for measuring the current.

To measure the pH (Fig. 2.9), a pH probe (Vernier, USA) with a BNC connector was used and the data were collected at each time period to make sure that the pH was staying

at around 6.7 all the time. The pH probe should be calibrated with pH buffer capsules each time before it is used to get the accurate data. Since dSpace accepts only voltage input, the value from the pH electrode to dSpace needed to be converted to the pH value through Nernst equation as mentioned before in Section 2.1.5.

Figure 2.9 The pH probe with BNC connector.

2.3.1 HPLC (High Performance Liquid Chromatography

HPLC is a method widely used in analytical chemistry. This method is a higher version of column chromatography, which is a method used for separation of individual chemical compounds from a mixture of compounds. HPLC does that with the aid of high pressure, with a much faster way of getting the results. The HPLC method was used to get the information for the acetate concentration in the substrate. Samples were taken from the MFC with a sterile syringe and was transferred to a centrifuge tube. These were centrifuged (the Reguera lab) to spin down the bacteria in the samples. The samples were reserved in a

Figure 2.10 dSpace CP1104.

freezer until the day they were analyzed. Acetate and metabolic end products in the sample supernatants were separated by high-performance liquid chromatography (Waters, Milford, MA) on a 300 by 7.8 mm Aminex HPX-87H column (Bio-Rad, Hrcules, CA) at 23°C with 4 mM H_2SO_4 as the eluent, at a flow rate of 0.6 mL/min [3].

Chapter 3

Microbial Fuel Cell Modeling

Microbial fuel cells, to describe simply, are devices that get energy from anaerobic digestion of the microorganisms. To develop a model for this behavior, one should understand the biological and electrochemical dynamics underlying the process. The biofilm model is important for understanding the electron transportation from the bacteria to the anode in mediator-less MFCs; however, the suspended microorganism model is the fundamental development for how the anaerobic digestion works and gives simpler approach for MFC modeling and control. In this study, the model of suspended microorganisms will be considered for simplicity; however, this approach can be extended to the biofilm model.

3.1 Microbial Kinetics

The connection between the active biomass and the primary substrates is the most fundamental factor needed for understanding. Because this connection must be made systematically and quantitatively for engineering design and operation, mass-balance modeling is an essential tool [16]. It is considered that the limiting factor for bacterial growth is the substrate (electron donor). The relation between these two dynamics is well known and captured by the Monod equation. Here, for a more systematic approach, we will consider the bacterial dynamics including both synthesis and decay. In the literature, usually when the researchers use biofilm model, instead of this approach, only synthesis part of bacterial dynamics is

considered and the decay rate is designed as the detachment rate from the biofilm. The rate of synthesis can be written as [1]

$$\mu_{\text{syn}} = \left(\frac{1}{X_{\text{a}}}\frac{dX_{\text{a}}}{dt}\right)_{\text{syn}} = \mu_{\max}\frac{S}{K+S} \tag{3.1}$$

X_{a} is the expression for the active biomass (for the our model, however, this will be written as X as it represents the total biomass in the system, considering that the bacteria are suspended), however, these kinetics can be approximated to describe the entire bacteria community due to the nature of suspended microorganisms. In this study, there will be no separation of active or inactive biomasses and the notation for all the suspended biomass is X.

On the other hand, as mentioned above, there will be bacterial decay. Studying more slowly growing bacteria has shown that active biomass has an energy demand for maintenance, which includes cell functions such as resynthesis and repair, motility, transport, osmotic regulation, and heat loss [1]. Environmental engineers usually represent that flow of energy and electrons required to meet maintenance needs as *endogenous decay* [16]. In other words, the bacteria oxidize themselves to meet those needs. The rate of endogenous decay can be represented as:

$$\mu_{\text{dec}} = \left(\frac{1}{X_{\text{a}}}\frac{dX_{\text{a}}}{dt}\right)_{\text{decay}} = -b \tag{3.2}$$

for $b > 0$, and b is endogenous decay coefficient.

Overall, the net specific growth rate of biomass (μ) is the sum of growth and decay rates:

$$\mu = \frac{1}{X}\frac{dX}{dt} = \mu_{\text{syn}} + \mu_{\text{dec}} = \mu_{\max}\frac{S}{K+S} - b \tag{3.3}$$

The substrate utilization is another kinetics worth to mention. The rate that bacteria break down the substrate is also related to the Monod equation. While the cell growth is derived from substrate utilization, the Monod equation takes the form [1]:

$$r_{\mathrm{s}} = -\frac{q_{\max} S}{K + S} X \tag{3.4}$$

where r_{s} is the rate of substrate concentration change (substrate utilization).

3.2 Growth Yield

The growth yield is a biological variable that allows us to assess the rate of electron-donor electrons converted to biomass electrons during synthesis of new biomass. Substrate utilization and biomass growth are connected by

$$\mu_{\max} = q_{\max} Y \tag{3.5}$$

where Y is called the growth yield.

The net rate of cell growth then becomes

$$X_{\mathrm{s}} = Y \frac{q_{\max} S}{K + S} X - bX \tag{3.6}$$

in which, X_{s} is the net rate of biomass growth. For modeling MFCs, the measured growth yield is beneficial. From (3.5), Y can be inferred from the two variables, $q_{\max}$ and $\mu_{\max}$. But it is useful to explain the direct measurement of Y. We can define the growth yield as the rate of bacteria concentration change divided by the rate of the substrate concentration

change. Then the growth yield takes a form,

$$Y = \frac{r_{\mathrm{x}}}{r_{\mathrm{s}}} \tag{3.7}$$

in which, r_{x} is the rate of bacteria concentration change (the net growth rate of biomass).

In batch systems, the growth yield becomes,

$$Y = -\frac{\frac{dX}{dt}}{\frac{dS}{dt}} = -\frac{dX}{dS} \tag{3.8}$$

Here, the minus sign comes from the equation (3.4) since the consumption rate of the substrate is a decreasing change.

For a continuous system, to calculate the growth yield, one could simply fix a time period and take the samples (for bacteria and substrate concentrations change) at initial and terminal times, and dividing them could give the approximate value of the growth yield,

$$Y = -\frac{\Delta X}{\Delta S} = -\frac{X - X_0}{S - S_0} \tag{3.9}$$

where ΔX is the bacteria concentration change in the fixed time period and ΔS is the substrate concentration change in that same fixed time period. X and S are the terminal bacteria concentration and substrate concentration, respectively. X_0 and S_0 are the initial bacteria concentration and substrate concentration, respectively.

3.3 Potential of an MFC

There is a difference between standard and non-standard electromotive forces of an MFC. If the cell is under standard conditions, the cell potential can be obtained by the difference between the standard electromotive force of the cathode and the standard electromotive force of the anode part in the MFC. Standard conditions are those that take place at

- T= 298.15 [K]
- P= 1 [atm]
- M_s= 1.0 [M]

where T is the temperature, P is the atmosphere pressure and M_s is the chemical concentration for liquid based on the IUPAC (International Union of Pure and Applied Chemistry) convention.

Non-standard conditions occur when any of these three conditions is violated, but generally they involve a change in concentration. The OCP of MFCs are based on the Nernst-Monod equation. Nernst-Monod equation is a quantitative expression that describes the relationship between the rate of ED utilization and two variables: ED concentration and electrical potential [35]. The standard potential of chemical reactions can be found in the literature [1], [18].

3.3.1 Thermodynamic Analysis

The reactions occurring in an MFC can be analyzed in terms of the half-cell reactions, or the separate reactions occurring at the anode and the cathode [18]. For example, the acetate

oxidization in the anode compartment can be represented as

$$CH_3COO^- + 4H_2O \Longrightarrow 2HCO_3^- + 9H^+ + 8e^- \tag{3.10}$$

whereas on the cathode side,

$$O_2 + 4H^+ + 4e^- \Longrightarrow 2H_2O \tag{3.11}$$

3.3.1.1 Activity

In chemical thermodynamics, activity is a measure of the effective concentration of species in a mixture, in the sense that the species' chemical potential depends on the activity of a real solution in the same way that it would depend on the concentration for an ideal solution [16].

Activity of a substance is a dimensionless value. The activity of pure substances in condensed phases (solids or liquids) is normally taken as unity (=1) [36]. For a reaction [36],

$aA+bB\leftrightarrow cC+dD$, where the left-hand side represents the reactants and the right-hand side represents the products, the reaction quotient has the form:

$$Q = \frac{[C]^c[D]^d}{[A]^a[B]^b} \tag{3.12}$$

where $[C]$ is understood to be the molar concentration of product C if it is aqueous, or the partial pressure in atmosphere if it is a gas.

Based on the chemical reaction involving the substrate on the anode side, we can calculate

the potential on the anode side E_{Anode}:

$$E_{\text{Anode}} = E_{0_{\text{a}}} - \frac{RT}{nF}\ln(Q) \tag{3.13}$$

in which, $E_{0_{\text{a}}}$ is the standard potential on the anode side. Standard potential is the potential under the standard conditions of those that were explained earlier in this section. R, T, n, F are the ideal gas constant, the temperature of MFC, the number of electrons transferred and the Faraday constant, respectively. The reaction quotient for the chemical reaction (3.10) which happens on the anode, will be,

$$Q = \frac{[CH_3COO^-]}{([HCO_3^-])^2([H^+])^9} \tag{3.14}$$

where CH_3COO^-, HCO_3^- and H^+ represent the acetate concentration, the bicarbonate ion concentration, and the proton concentration, respectively. In the same manner, we can calculate the potential on the cathode side based on the chemical reaction there,

$$E_{\text{Cathode}} = E_{0_{\text{c}}} - \frac{RT}{nF}\ln(Q) \tag{3.15}$$

in which, $E_{0_{\text{c}}}$ is the standard potential on the cathode side.

Thus, the overall potential of an MFC can be calculated as,

$$E_{\text{Cell}} = E_{\text{Cathode}} - E_{\text{Anode}} \tag{3.16}$$

3.4 Voltage Output

In the previous section, the potentials described in the Eqs. (3.13)-(3.16) are theoretical calculations depending on the chemical reactions happening in the MFC. The measured voltage of an MFC will be lower than this value due to the potential losses, as explained below.

3.4.1 Activation Losses

The activation loss occurs at the beginning of the process of the system. Because a chemical reaction needs to be activated to start, activation loss occurs during the transfer of the electrons from the bacteria to the anode. The activation loss at each electrode of a fuel cell is governed by the Butler-Volmer equation [49],

$$I_{\mathrm{MFC}} = i_0 A_{\mathrm{sur}} [\exp(\frac{\beta_1 - nFV_{\mathrm{act}}}{RT}) - \exp(-\frac{\beta_2 - nFV_{\mathrm{act}}}{RT})] \tag{3.17}$$

where I_{MFC} is the MFC current, i_0 is the exchange current density in reference conditions, A_{sur} is the anode surface area, and V_{act} is the activation loss (the loss is in terms of potential since it is taken from the total voltage on the electrode) on the anode. The reduction (β_1) and oxidation (β_2) transfer coefficients are determined by the electron transfer processes at the electrode-electrolyte interface [39]. These coefficients are directly related to the electrode reaction mechanism and are difficult to identify [49]. The exchange current density in reference conditions is a strong function of electrode materials, design, reactant and product concentrations, and temperature [39]. Eq. (3.17) can be reduced to the Tafel equation for

large values of activation losses,

$$V_{\text{act}} \approx \frac{RT}{\beta nF} \ln\left(\frac{I_{\text{MFC}}}{i_{0\text{ct}} A_{\text{sur}}}\right) \tag{3.18}$$

For small values of V_{act}, Eq. (3.17) can be reduced to a linear relationship between the current and the activation loss. This reduction is often called "linear current-potential equation" as shown in [60], [39],

$$V_{\text{act}} \approx \frac{RT}{nF} \left(\frac{I_{\text{MFC}}}{i_0 A_{\text{sur}}}\right) \tag{3.19}$$

It must be noted that, [49] has clearly demonstrated that Butler-Volmer approximations leading to the Tafel and linear current-potential equations should be cautiously used in modelling and model analysis, because they could significantly deviate from the Butler-Volmer equation outside their range of applicability [39].

3.4.2 Ohmic Losses

Resistance to the flow of electrons and ions during the fuel cell operation generates ohmic losses. These losses increase as the current flow increases and this linear relationship obeys Ohm's law; therefore, ohmic losses can be described by [6]:

$$V_{\text{ohm}} = R_{\text{int}} I_{\text{MFC}} \tag{3.20}$$

where V_{ohm} and R_{int} are ohmic loss on the anode side and the internal resistance of MFC, respectively.

Ohmic losses arise from resistance of ion (proton) conduction due to the solution and

(if present) the membrane, and resistance of the flow of electrons from the electrode to the contact point (i.e., where the electrodes are connected to a wire), and any relevant internal connections. Ohmic losses can be limited by reducing electrode spacing, choosing membranes or electrode coatings with low resistances (if present), ensuring good contacts between the circuit and electrodes, and increasing solution conductivity and buffering capacity [18].

3.4.3 Concentration Losses

The concentrations of the reactants and products in the fuel cell at the compartment bulk phase are often different from their concentration values at the electrode surface. Due to consumption and formation reactions, reactants are sparse at the electrode surface, while products are abundant. This concentration gradient leads to a mass transport phenomenon that is determined by diffusion. Since the current produced by the fuel cell is linked to the electrode reactions, the diffusion of reactants and products affects the fuel cell performance. This influence is called concentration losses [39].

The concentration losses contribute significantly to the decrease in cell potential, particularly at high current densities and low bulk reactant concentrations [49], [39]. These losses can be determined by the potential difference (ΔE) between the voltage at open circuit (bulk concentration, $E_{i=0}$) and the cell voltage at high current rates ($\mathrm{E_{i-high}}$) [6]. So, the Nernst equation can be applied between the reactants' concentrations in the bulk liquid (C_{Bulk}) and on the electrode surface (C_{Surface}) as:

$$\Delta E = V_{\mathrm{conc}} = \frac{RT}{nF}\ln(\frac{C_{\mathrm{Bulk}}}{C_{\mathrm{Surface}}}) \tag{3.21}$$

In addition, one can define $I_{\mathrm{L}}^{\mathrm{R}}$ as the limiting reference current, e.g., the maximum

possible current density, at which the maximum rate of reactants can be supplied to the electrode. By this definition, C_{Surface} is zero at I_{L}^{R}. Now by applying Fick's law at the limiting reference current and by using eq. 3.21 one can find [6], [39],

$$\frac{C_{\text{Bulk}}}{C_{\text{Surface}}} = \frac{I_{\text{L}}^{\text{R}} - I_{\text{MFC}}}{I_{\text{L}}^{\text{R}}} \tag{3.22}$$

Therefore, the concentration losses can be written as a function of fuel cell current and its limiting reference current [39],

$$V_{\text{conc}} = \frac{RT}{nF}\ln(1 - \frac{I_{\text{MFC}}}{I_{\text{L}}^{\text{R}}}) \tag{3.23}$$

3.4.4 The Voltage Output

Based on the previous discussions, the measured potential on the anode electrode,

$$V_{\text{Anode}} = E_{\text{Anode}} - [V_{\text{act}} + V_{\text{ohm}} + V_{\text{conc}}] \tag{3.24}$$

For the cathode potential, the same procedure can be applied; however, in this study, the cathode potential is assumed to be constant. The assumption of constant cathode potential comes from the main attention on the anode potential output [48].

3.5 A Control-oriented Model for MFCs

In this section, the mathematical model developed for the purpose of controller design is summarized in a form that clearly indicates state variables, control input, and outputs. A control volume is described as a mathematical abstraction to help build the mathematical

models of physical processes (chemical reactions in this study). In the continuous (or fed-batch) mode, MFCs can be perceived as chemostats (a control volume which includes the organic matter and the microorganism). In this chemostat the input and the output are controlled for the desired purposes. The proposed model considers only one kind of microorganism and uses acetate as the substrate, but the approach is amenable to generalization to a mixture of microorganisms and other types of substrates. The following assumptions are made in the model development:

1. The mixing of substrate is ideal, and the substrate gradient in the biofilm is neglected.

2. the substrate concentration change is the main effect on the anode OCP output.

3. The temperature remains constant at the room temperature, and the pH is kept constant via the pH buffer in the medium.

4. The main overpotential affecting the cathode potential is the activation loss. For simplification and because of the small changes in the cathode OCP, the cathode OCP is assumed constant [48].

5. There is no manual addition of active biomass to the system.

3.5.1 Mass Balances

Describing mass balances and the rate of substrate concentration change requires specifying a control volume. In Section 3.1, the concentrations of bacteria and the substrate in the batch mode (closed volume) are discussed. In this section, the input to the control volume is included in the state equations. The liquid volume of the MFC is denoted as V_{c}. The system receives a feed flow with rate F_{c}, having initial substrate concentration of S_0, which

described as the MFC initial substrate concentration before. This substrate feed is coming from the substrate storage container (Fig. 2.1). The storage container has the substrate concentration of S_0, so it feeds the MFC container with that value. The rate of change in substrate concentration in the MFC is,

$$\frac{dS}{dt} = -qX + D(S_0 - S) \tag{3.25}$$

The dilution rate, D, is the control input to the system. By changing the value of D, one can examine the flow rate effect on the output of the MFC since the dilution rate is a function of the flow rate,

$$D = F_{\mathrm{m}} V_{\mathrm{m}}^{-1} \tag{3.26}$$

In Eq. (3.25), q is related to r_{s} in (3.4),

$$q = q_{\max} \frac{S}{K + S} \tag{3.27}$$

In the continuous (or fed-batch) system, the biomass mass balance equation is,

$$\frac{dX}{dt} = \mu X - DX \tag{3.28}$$

Again, the parameter μ represents the net specific growth rate of the bacteria.

3.5.2 Summary of the Control-oriented Model

3.5.2.1 State Equations

To facilitate the discussion on the analysis of the MFC dynamics, we introduce new notation for the dynamics that is more commonly used in the control literature. Let x_1 represent the substrate concentration (the original S) and x_2 represent the biomass concentration (the original X). The input, u, represents the dilution rate, D. The system dynamics can be represented as

$$\dot{x_1} = -q_{\max}\frac{x_1}{K+x_1}x_2 + u(S_0 - x_1) \tag{3.29}$$

$$\dot{x_2} = [\mu_{\max}\frac{x_1}{K+x_1} - b - u]x_2 \tag{3.30}$$

$$\dot{x_3} = 2(q_{\max}\frac{x_1}{K+x_1}x_2 - u(S_0 - x_1)) \tag{3.31}$$

$$\dot{x_4} = 9(q_{\max}\frac{x_1}{K+x_1}x_2 - u(S_0 - x_1)) \tag{3.32}$$

where new state variables x_3 and x_4 are the new representations of HCO_3^- and H^+ concentrations, respectively. The significance of these concentrations in the voltage output is explained in Section 3.3.1.1. The reason for these state variables chosen that way (Eqs. (3.31), (3.32)) is due to the chemical reaction that happens on the anode side; see (3.10). The change of the activity for x_3 and x_4 is assumed not to affect the acetate concentration equation, because the system is closed and there is no transfer of ions in or out of the system.

3.5.2.2 Output

Depending on the configuration of the MFC measurement setup, there are multiple ways for defining the system output. Before writing the control-oriented OCP output, all the parameters in the equation should be written in terms of state variables, constant parameters and the inputs. One common and convenient choice for the output is the open-circuit voltage:

$$V_{\text{Anode}} = E_{0_{\text{a}}} - \frac{RT}{nF}\ln(x_1/(x_3^2 x_4^9)) - [\frac{RT}{nF}(\frac{I_{\text{MFC}}}{i_0 A_{\text{sur}}}) + R_{\text{int}} I_{MFC} + \frac{RT}{nF}\ln(1 - \frac{I_{\text{MFC}}}{I_{\text{L}}^{\text{R}}})] \quad (3.33)$$

This equation comes from Section 3.4 with activation, ohmic and concentration losses subtracted from the theoretically calculated OCP of anode.

To be able to estimate the internal resistance, the following equation can be used [39],

$$R_{\text{int}} = R_{\text{MIN}} + (R_{\text{MAX}} - R_{\text{MIN}})e^{-K_R X} \quad (3.34)$$

Again, X is the biomass concentration and will be denoted as x_2 as mentioned before..

Another variable that should be written in terms of the state variables is I_{MFC}. In the study [37], the authors defined the current density:

$$j = j_{\max}\frac{S}{K+S} \quad (3.35)$$

where S and K are the same as before, the substrate concentration and the concentration giving one-half the maximum rate, respectively, j is the current density on the anode part

and j_{max} is the maximum current density obtained on the anode part. This definition, however, was based on the region of bulk substrate concentration in a biofilm model. So, this definition is approximated in this study for the bulk substrate concentration. Since the current density is the current divided by the surface area (anode surface area in this case), then the current becomes,

$$I_{\mathrm{MFC}} = A_{\mathrm{sur}} j_{\max} \frac{S}{K+S} \tag{3.36}$$

or,

$$I_{\mathrm{MFC}} = A_{\mathrm{sur}} j_{\max} \frac{x_1}{K+x_1} \tag{3.37}$$

Then Eq. (3.33) becomes,

$$\begin{aligned} V_{\mathrm{Anode}} = E_{0_{\mathrm{a}}} - \frac{RT}{nF}\ln(x_1/(x_3^2 x_4^9)) - [\frac{RT}{nF}(\frac{j_{\max}\frac{x_1}{K+x_1}}{i_0}) \\ + (R_{\mathrm{MIN}} + (R_{\mathrm{MAX}} - R_{\mathrm{MIN}})e^{-K_R x_2}) A_{\mathrm{sur}} j_{\max} \frac{x_1}{K+x_1} \\ + \frac{RT}{nF}\ln(1 - \frac{A_{\mathrm{sur}} j_{\max}\frac{x_1}{K+x_1}}{I_{\mathrm{L}}^{\mathrm{R}}})] \end{aligned} \tag{3.38}$$

3.6 Experimental Model Identification

3.6.1 OCP Measurement

Model identification was conducted using the data from the first experiments for both the cases of 3 mM and 1 mM acetate operated in the batch mode and from the HPLC results. Matlab simulation results were used to figure out the confidence intervals for the estimated parameters. For the data collection, first the MFC was inoculated with 3 mM acetate and 10 mL of bacteria culture with a concentration of $5\text{x}10^{10}$ cells/mL initially. The maximum

open circuit potential (OCP) of the anode was observed to be −471 mV (Fig. 3.1) and its magnitude was decreasing afterwards (Fig. 3.2).

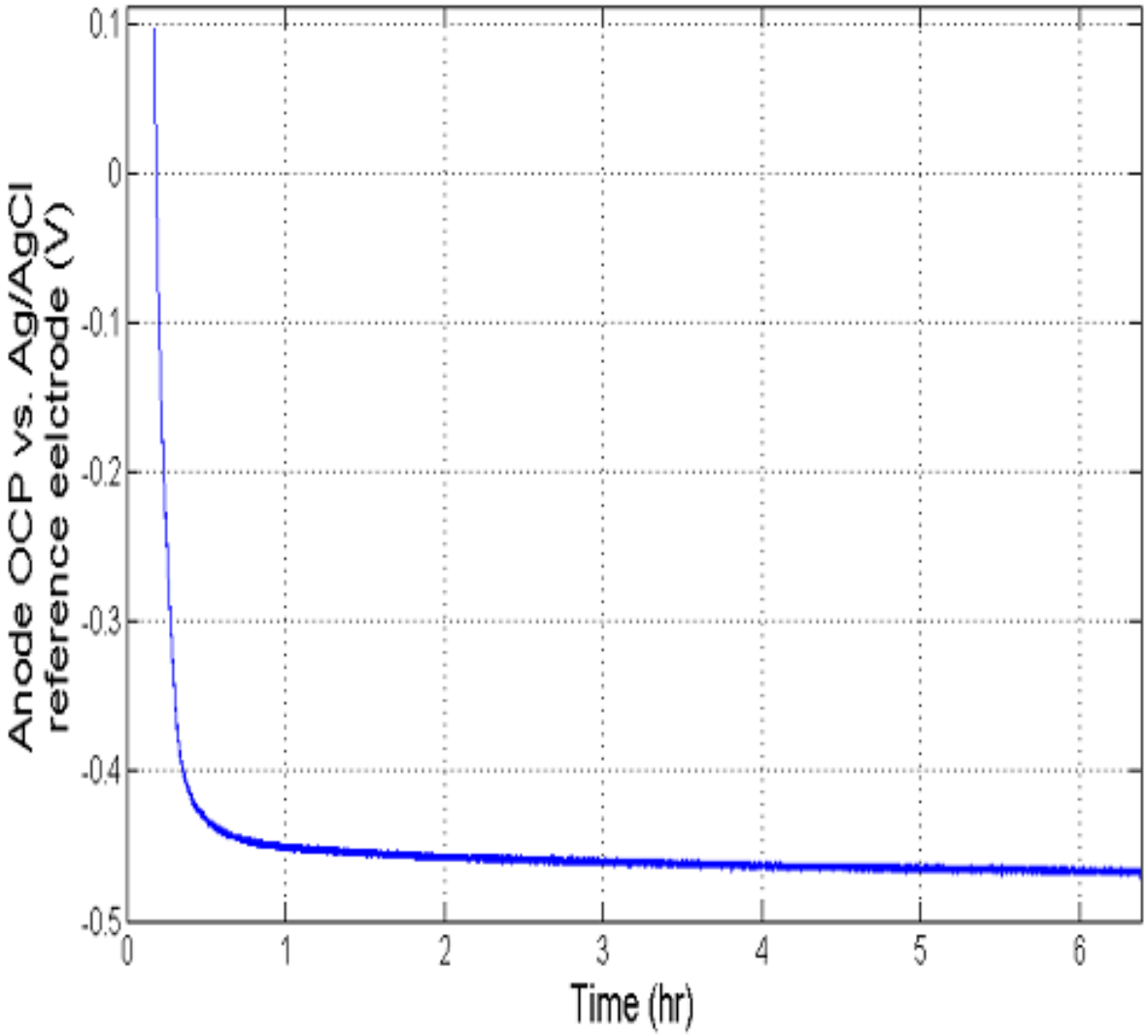

Figure 3.1 Anode open circuit potential versus Ag/AgCl reference electrode after the bacteria inoculation.

For the second experiment, the MFC was inoculated with 1 mM acetate and the same volume and density of bacteria initially. The maximum OCP of the anode was observed to be −362 mV and similarly it was decreasing afterwards. The identifiable parameters from the OCP and HPLC results were, $\mu_{\max}$ and $q_{\max}$. There are some parameters that are

difficult to identify, for which we have used the data from the literature to determine their values.

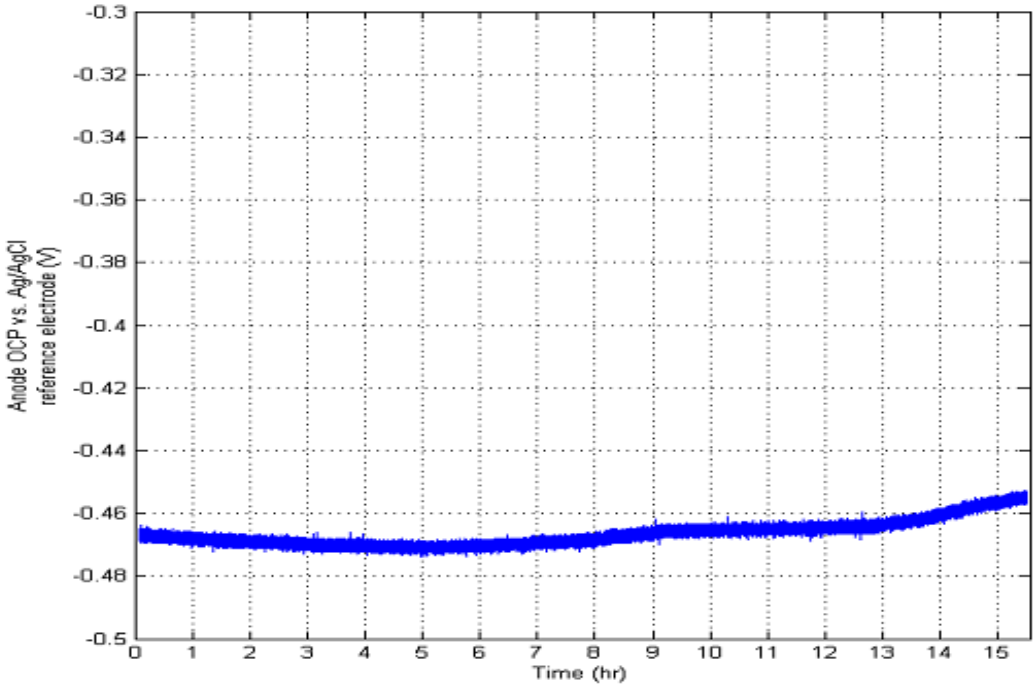

Figure 3.2 Maximum point of anode OCP versus Ag/AgCl reference electrode. The OCP of anode was decreasing after that point.

For the estimation of those identifiable parameters, data-fitting was carried out. Basically, the best values for the parameters were chosen based on the values gathered from the OCP values for the substrate concentration (x_1). This value then was also validated with the HPLC analysis results. Because running too many experiments was not available in this study, the data from the literature was used to identify the other parameters (ones that are not identifiable with the current experimental data). The identification of several parameters present in the OCP equation requires additional experiments such as cyclic voltammetry and polarization tests with different external resistors; however, in this study, these experiments were not conducted yet. The parameters estimated for our system are listed in Table 3.1.

3.6.2 HPLC Measurement

The acetate concentration initially was 1 mM (59 mg/L). This initial condition was used in Matlab/Simulink simulation of the model. Simulation suggests that almost 63% of the acetate was consumed (Fig. 3.3) by the bacteria in 6 days and that result agreed with the HPLC result which was taken after 6 days the inoculation was done. The HPLC results showed that the acetate concentration was 0.38 mM on 6th day.

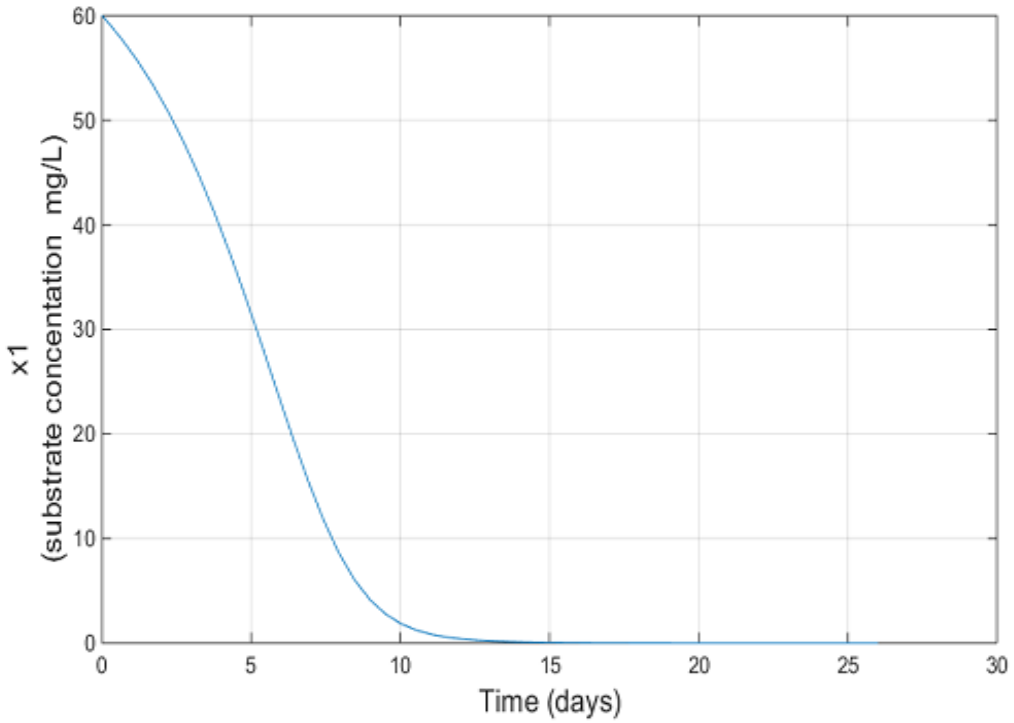

Figure 3.3 The simulation results for the acetate concentration change with zero input (batch mode).

The parameters such as R, and F are universal constants with known values. The value for T, was taken as 298.15 K which is the temperature of the room in the MFC and is assumed to stay unchanged. The anode surface area was calculated approximately by measuring the dimensions of the anode brush (0.67 m^2). The electrons per chemical reaction is 8 e^- which is known from (3.10). The value for E_{0_a} (0.187 mV), which is the anode

Table 3.1 Parameters identified for the MFC model.

Parameter	**Description**	**Value**	**Unit**	**Explanation**
$q_{\max}$	maximum specific rate of substrate utilization	3	day^{-1}	estimated
K	concentration giving one-half the maximum rate	27	mg L^{-1}	assumed
$\mu_{\max}$	maximum specific growth rate	0.5	day^{-1}	estimated
S_0	initial acetate concentration	60	mg/L	known
X_0	initial bacteria concentration	1.5	mg/L	known
F	Faraday constant	96485	s A/mol	constant
R	ideal gas constant	8.31446	$\text{JK}^{-1}\text{mol}^{-1}$	constant
T	MFC temperature	298.15	K	constant
n	number of electrons transferred	8	dimensionless	known
b	endogenous decay coefficient	0.07	day^{-1}	estimated
E_{0_a}	standard anode potential	0.187	V	constant
A_{sur}	Anode surface area	0.67	m^2	calculated

OCP under the standard conditions, was taken from the literature [4], [18]. This value has already been calculated before, according to the chemical reaction (3.10) that happens in the anode part with the acetate as the substrate. The values for $\mu_{\max}$, b (the endogenous decay coefficient), and $q_{\max}$ were estimated by using the OCP and HPLC data from the experiments via data fitting method (Table 3.1). The value for K is the least predictable value. This non-identifiable parameter was taken from the literature [1], [35], [58] based on the similar operating conditions.

3.6.3 pH measurement

For the pH measurement, the pH electrode with the BNC connector was used. The samples for the pH values were taken from the MFC bottle with a sterilized syringe twice everyday with approximately 12 hours intervals. The calibration for the pH electrode was made manually as described before in Section 2.1.5.1. The calibration for the pH electrode was needed everyday. As it can be seen in Fig. 3.4, the pH did not change significantly due to the pH buffer in the solution (potassium phosphate).

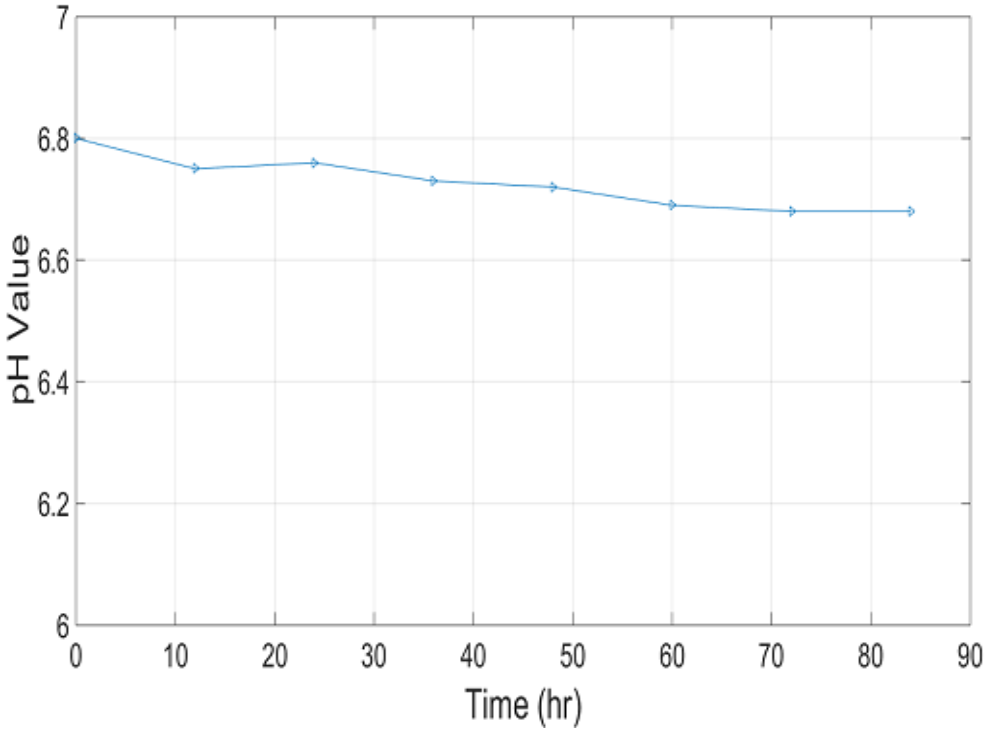

Figure 3.4 The pH values taken twice a day.

3.7 Model Validation

Model validation has been done using 1 mM acetate concentration and the $5x10^{10}$ cells/mL, and we had 10 mL bacteria culture which means that there was $5x10^{11}$ cells initially in the

MFC. For the simulation part, the x_3 and x_4 initial values were taken as zero since they are assumed to be absent until the bacteria starts consuming organic matter. The values for the x_3 and x_4 are linearly dependent on x_1 in the model proposed in this study. With this simulation, the result for 1 mM acetate concentration is shown in Fig. 3.5.

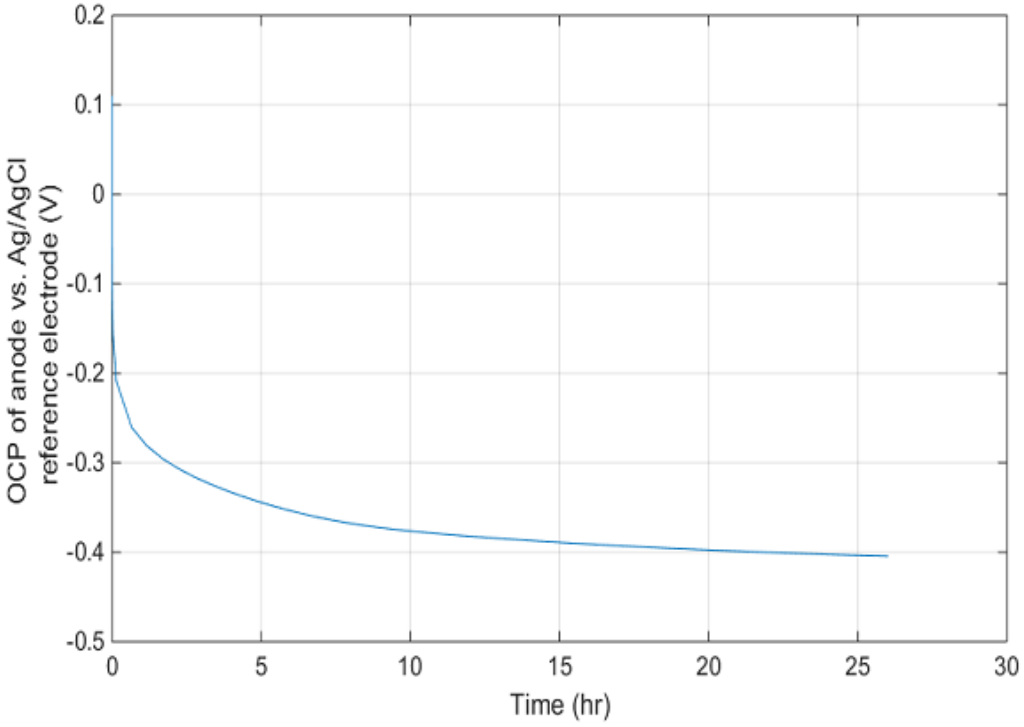

Figure 3.5 Simulation results for the anode open circuit potential versus Ag/AgCl reference electrode after the bacteria inoculation.

The MFC had 220 mL medium bubbling with N_2 for 5 hours before the bacteria inoculation. The OCP of the anode was observed to be +112 mV at that time. Then 10 mL of the bacteria inoculation was added and the OCP of anode started increasing drastically. The OCP that was observed on the anode side was −380 mV in 2.5 hours after the bacteria were added (Fig. 3.1). Then the observation showed that in 60 hours the magnitude of OCP of the anode went down to −320 mV (Fig. 3.6). Note that, because of the dSpace converting the voltage value sign from the potantiostat, the signs of the voltage values seem to have

flipped.

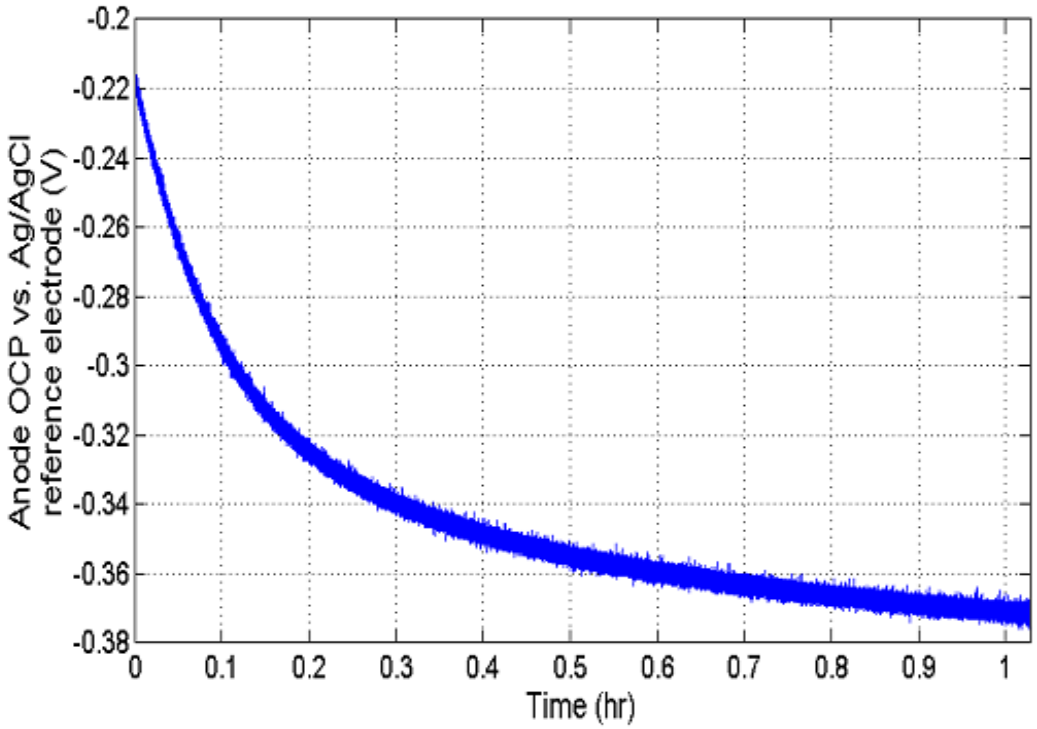

Figure 3.6 Anode open circuit potential versus Ag/AgCl reference electrode after the bacteria inoculation.

Based on the model, we have conducted additional simulation analysis. For the initial bacteria concentration, it has been estimated to be $5\text{x}10^{13}$ cells/mL. With one bacterium mass weight of $3\text{x}10^{-17}$ g [64], the initial bacteria mass concentration following inoculation was estimated to be 1.5 mg/L (Fig. 3.7). The bacteria concentration reached the maximum level in 7 days and it started decreasing due to the depleting acetate concentration. However, simulation results showed that the bacteria concentration did not reach to zero even in 20 days after the substrate concentration was almost zero. It is because the bacterial endogenous decay coefficient in the Eq. (3.7) was small.

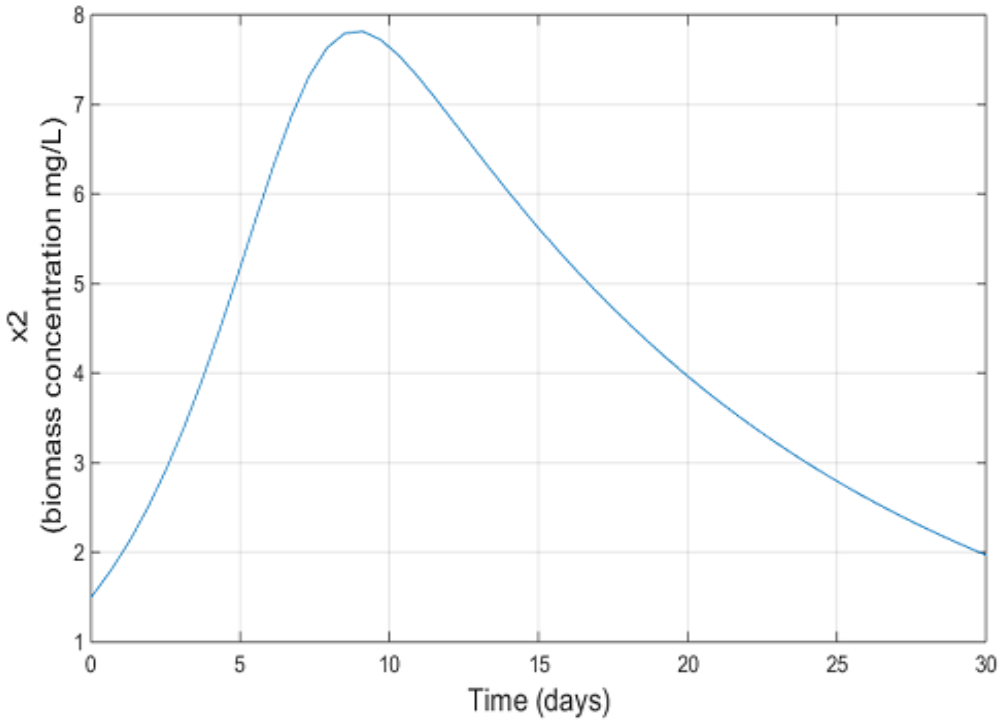

Figure 3.7 The simulation results for the bacteria concentration change with zero input (batch mode).

Chapter 4

MFC Model Analysis

In this chapter, the MFC model will be analyzed in the fed-batch (where either $u = 0$ or a constant) and continuous mode (u can be changed). For the continuous mode, we restrict to the case of u being constant. First, the equilibria of the system will be investigated and the properties of these equilibrium points will be studied. We will further explore the bifurcation of the system behavior as the (quasi)constant control input u increases. Stability of these equilibria will also be analyzed.

4.1 Equilibria of the System

It is important to understand the properties of the system dynamics in an MFC, which will be instrumental in the MFC control and optimization. One important property is the set of equilibria and their stability. Recall the state equations (3.29 - 3.32). The first two state equations will be considered in this chapter to analyze the behavior of the substrate and the biomass concentration.

From the second equation of the state equations, there is a trivial equilibrium point,

$$x_2 = 0 \quad \Rightarrow \quad x_1 = S_0 \tag{4.1}$$

which means that if there is no bacteria, the substrate concentration will remain constant

regardless of the input value. The other equilibrium point is when x_1,

$$x_1 = \frac{K(b+u)}{\mu_{\max} - b - u} \tag{4.2}$$

then the corresponding x_2 is

$$x_2 = \frac{\mu_{\max} u(Kb + S_0 b + Ku - S_0 \mu_{\max} + S_0 u)}{q_{\max}(b+u)(b - \mu_{\max} + u)} \tag{4.3}$$

The latter is the nontrivial equilibrium point, which depends on the input value. The importance of the dilution rate (the input) could be seen in this equilibrium in a continuous-mode MFC. From this equilibrium expression, we note that if $u = \mu_{\max} - b$, no finite equilibrium can be achieved.

A special case of interest is when $u = 0$ (the fed-batch mode). In that case, one of the eigenvalues becomes zero. When one or both eigenvalues are zero, the phase portrait (the family of all trajectories) is in some sense degenerate [2]. When that situation happens, there is a null space, any vector in which is an equilibrium point for the system; that is, the system has an equilibrium subspace, rather than an equilibrium point. In Fig. 4.1, this subspace can be seen with the red marks on the phase portrait. Depending on the initial conditions for the bacteria and the substrate concentrations, an equilibrium will be reached in the equilibrium subspace. In this case, the equilibrium space is $x_2 = 0$ and x_1 can take any positive number but K (concentration giving one-half the maximum rate).

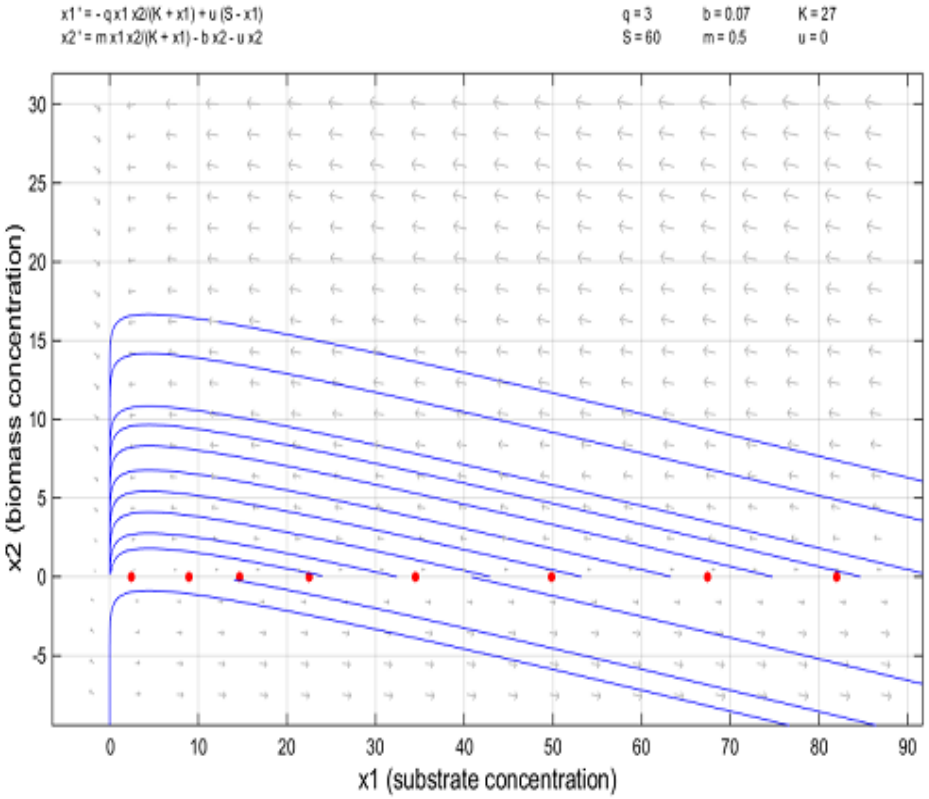

Figure 4.1 The phase portrait for the equilibrium subspace with zero input (fed-batch mode).

4.2 Stability of the Equilibria

Consider the nonlinear time-invariant system (Eqs. (3.29 - 3.32)). We analyze the local stability through linearization at the equilibrium point of interest. In particular, the Jacobian matrix is,

$$J = \begin{bmatrix} \frac{-Kq_{\max}x_2}{(K+x_1)^2} - u & \frac{-q_{\max}x_1}{K+x_1} \\ \\ \frac{K\mu_{\max}x_2}{(K+x_1)^2} & \frac{\mu_{\max}x_1}{K+x_1} - b - u \end{bmatrix} \tag{4.4}$$

At the first trivial equilibrium point, $x_2 = 0$ and $x_1 = 60$, with the values from the Table 3.1, the J matrix is,

$$J = \frac{\partial f}{\partial x} = \begin{bmatrix} -u & -2.069 \\ \\ 0 & 0.275 - u \end{bmatrix} \tag{4.5}$$

Since $u \in \mathrm{R}^+$, unless $u \leq 0.275$, the equilibrium point is locally asymptotically stable because both the eigenvalues are real and negative. However, something interesting happens when the dilution rate reaches one specific value, when $u = 0.275$, one of the eigenvalues $\lambda_1 = -11/40$ and the other eigenvalue $\lambda_2 = 0$, which gives another nullspace. On the other hand, when $u < 0.275$, one of the two eigenvalues is negative while the other is positive. In that case this equilibrium point is called a saddle point and it is not stable.

The second equilibrium point of Eqs. (4.2)-(4.3) is more important since it is more

practically relevant. The J matrix for a constant u becomes,

$$J = \begin{bmatrix} -\frac{u(290000u^2-159400u+37421)}{450(100u+7)} & -6u-\frac{21}{50} \\ \\ \frac{u(290000u^2-204400u+34271)}{2700(100u+7)} & 0 \end{bmatrix} \tag{4.6}$$

For this matrix, the eigenvalues as a function of u are calculated,

$$\begin{aligned} \lambda_1 = -(37421u + (u(84100000000u^5 - 144652000000u^4 + 76596540000u^3 \\ - 13203494800u^2 + 716982841u - 30227022))^{1/2} \\ - 159400u^2 + 290000u^3)/(900(100u+7)) \end{aligned} \tag{4.7}$$

$$\begin{aligned} \lambda_2 = -(37421u - (u(84100000000u^5 - 144652000000u^4 + 76596540000u^3 \\ - 13203494800u^2 + 716982841u - 30227022))^{1/2} \\ - 159400u^2 + 290000u^3)/(900(100u+7)) \end{aligned} \tag{4.8}$$

Using Matlab, the eigenvalues for increasing u from zero to 0.3 by 0.01 increment calculated. The plotted eigenvalues for these different u values are as shown in Fig. 4.2.

An interesting phenomenum, called bifurcation, is important in the practical sense. It is whether the system maintains its qualitative behavior under infinitesimally small perturbations [2]. In this control model the input changes to a specific value and the non-trivial equilibrium point changes its stability property at a certain input value. With the parameters in Table 3.1, this input value is $u = 0.275$. This is the same input value with the previous case. That interesting result shows us that both these two equilibrium points (Eqs. (4.1)

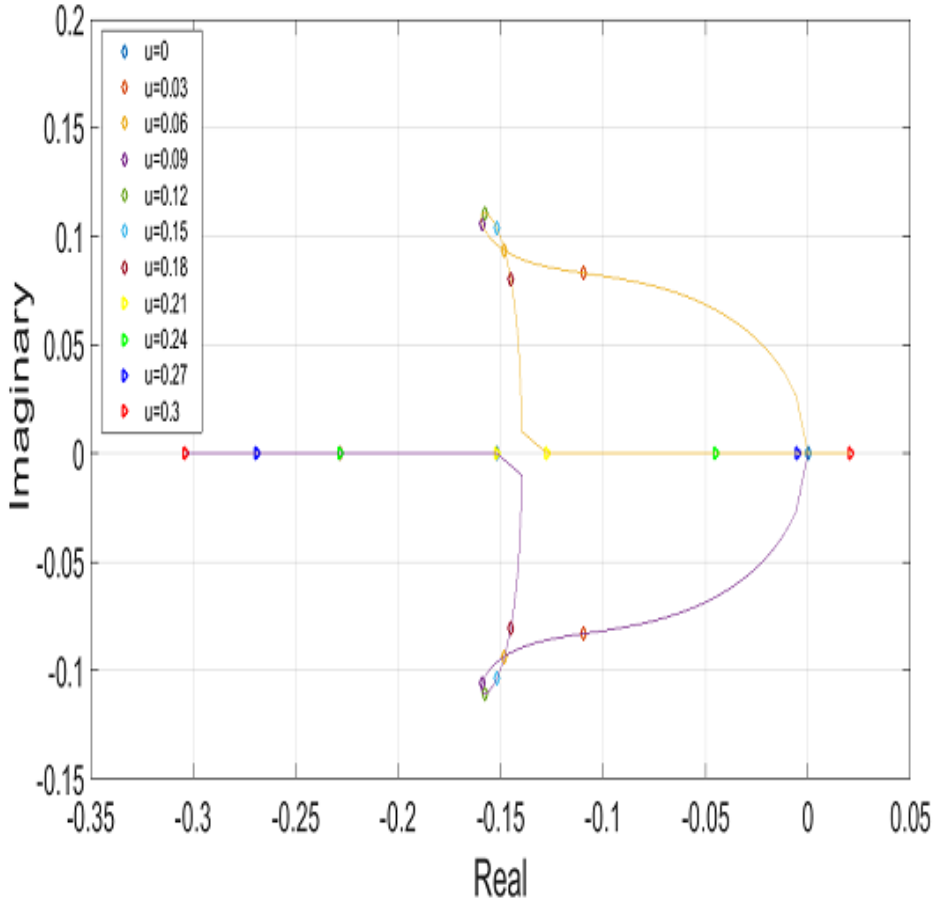

Figure 4.2 The eigenvalues for different u values to show the bifurcation point. The orange line shows the trajectory of the first eigenvalue and the purple line shows the trajectory of the second eigenvalue.

and (4.2, 4.3)), are changing their property at that specific u value. Our interest is mainly on the first equilibrium point (Eq. (4.1)) since the second equilibrium point goes beyond the physical domain. The first equilibrium point becomes locally asymptotically stable. This result suggests that after the specific u value, the washout will happen. In Fig. 4.2, until around the value $u = 0.2$, eigenvalues are complex and in the graph, only the real part of the eigenvalues is considered since it is deciding the stability property. After that u value, there is another u value, $u = 0.275$, at which, it is easy to see that the first eigenvalue is switching its sign (while the other remains at negative), which causes a bifurcation at that point (from stable to saddle).

The linearized system at the second equilibrium point (Eq. (4.6)) strictly depends on u. For $0 < u < 0.275$, the point is a stable node because the real parts of the two eigenvalues of the Jacobian matrix are negative. When $u = 0.275$, the two equilibrium points are colliding and one of the equilibrium points changes the stability property. This second equilibrium point becomes a saddle point due to one negative and one positive eigenvalue of the matrix. Besides, theoretically, after that $u = 0.275$ value, this second equilibrium point is going beyond the domain which is $x_1 \in D$, $x_2 \in D$, $D \in \mathrm{R}^+$. This case can be shown in phase portraits and also can be seen in Matlab/Simulink simulation for different u values. Here, for $u = 0.2$, the stable equilibrium point is $x_1 = 31.69$ and $x_2 = 3.49$ (Fig. 4.3). For $u = 0.3$, the equilibrium point becomes a saddle point due to bifurcation.

Simulation results for different u values are shown in Fig. 4.5, to show how substrate and bacteria concentrations change and stabilize, which agrees with the previous analysis.

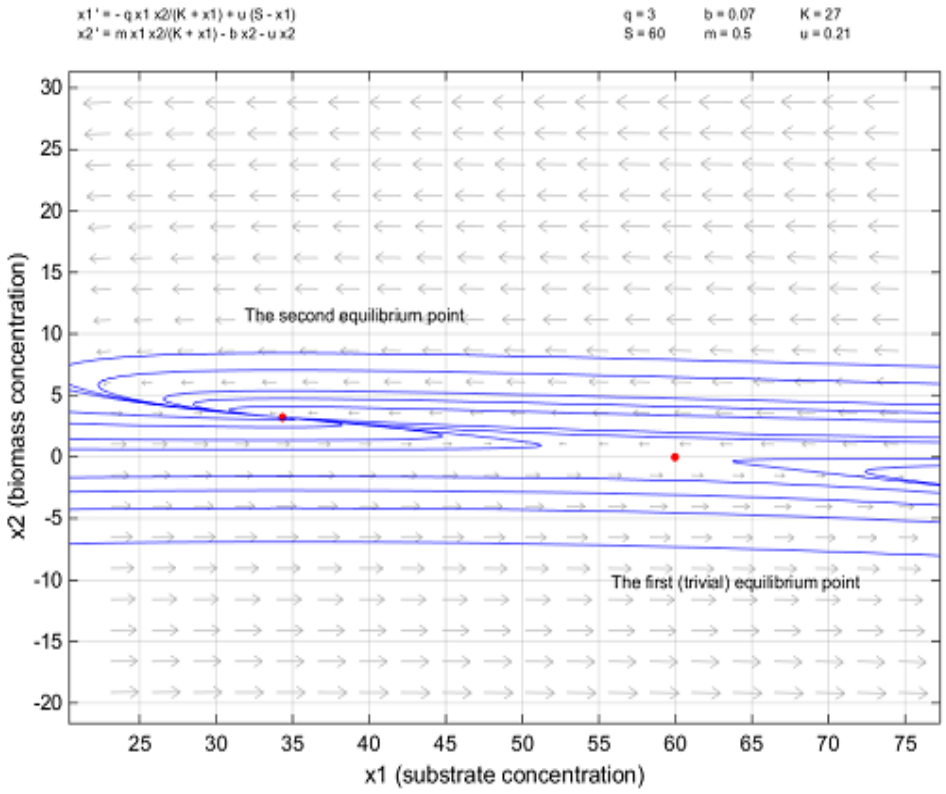

Figure 4.3 The phase portrait for the second equilibrium point with non-zero input value, 0.2.

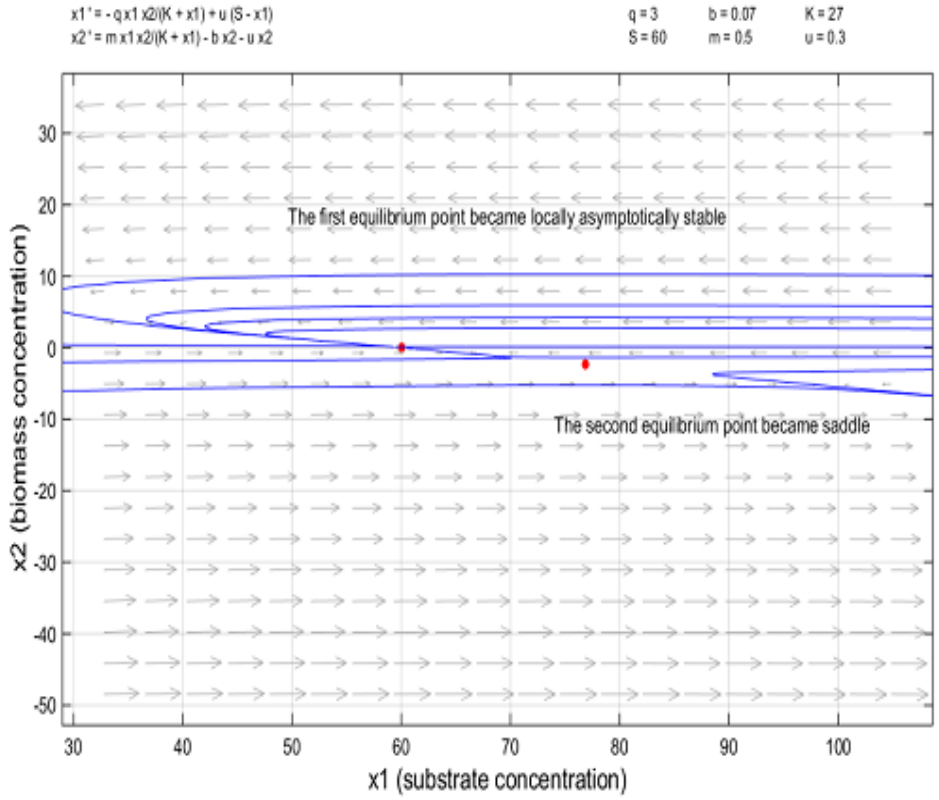

Figure 4.4 The phase portrait for the second equilibrium point with non-zero input value, 0.3.

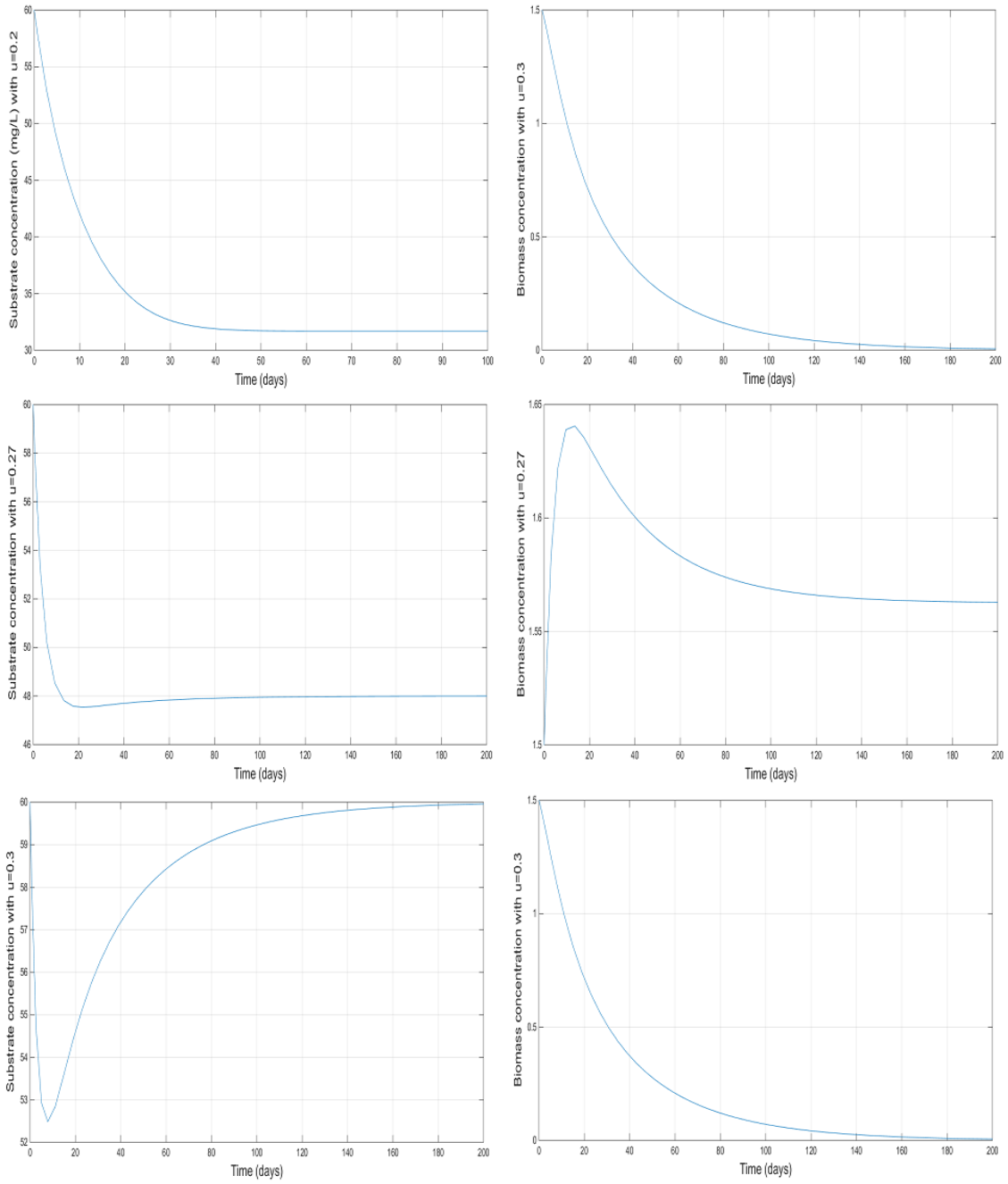

Figure 4.5 Substrate and biomass concentration stabilization with the change of the dilution rate.

Chapter 5

Conclusion and Future Work

5.1 Conclusion

The main contribution of this thesis is to develop a model for a microbial fuel cell based on the anaerobic digestion conduct model validation with the support from the experimental data results, and perform analysis of this model based on the nonlinear systems theory.

The model for the MFC was chosen based on the suspended bacteria assumption. The kinetics for the substrate consumption and the bacterial growth were taken from the literature. However, for the ions and protons activity, changes were put in the differential equations based on the chemical reaction. The model was not adequate for supporting the experimental results perfectly. This indicates that the biofilm kinetics must be included for the MFC without mediator. The experiments were carried out with anaerobic pure culture for the bacteria, acetate as the substrate, and membrane-less single-chamber as the MFC structure. Identifiable parameters for the model were estimated using data from the experiments in the batch mode. Non-identifiable parameters were carefully chosen from the literature. The model validation was conducted with the independent data sets and this assured that the model could simulate the state variables as well as the output. The simulated open circuit potential output was slightly higher than the measured open circuit potential of the anode. This was because the model did not include the crossover potential loss.

The model analysis was conducted after the model was validated. Similar anaerobic

digestion analysis was conducted before by other researchers; however, for MFCs, this kind of analysis has not been done before. The stability of the equilibria under the continuous mode was examined, and the results showed that there is a good dilution rate interval. The biomass will theoretically be washed out with the input value higher than the threshold, which was calculated after the analysis. However, in a biofilm-based model this would not be true completely because of the detachment to the biofilm. This analysis, however, could be used on the suspended portion of the bacteria contribution on the voltage output.

5.2 Future Work

The future work can be mainly concentrated on a better model development. The model parameters identification in this study was carried out with limited measurements from the experiments. The tests such as polarization, cyclic voltammetry, electrochemical impedance spectroscopy may give important data for more accurate parameter identification.

State variables, such as the substrate and the bacteria concentrations can potentially be estimated by using extended kalman filtering. Ultimately, with the estimated states, feedback control of the MFC can be pursued, to stabilize or maximize the power output for the MFC system.

BIBLIOGRAPHY

BIBLIOGRAPHY

[1] Rittmann B. E., and McCary P. L., (2001). *Environmental Biotechnology: Principles and Applications*. McGraw-Hill Education, Columbus, OH, USA.

[2] Khalil H. K., (2002). *Nonlinear Systems*. Third edition, Pearson Education, Inc., Prentice Hall, Upper saddle River, NJ, USA.

[3] Speers A. M., and Reguera G., (2012). *Electron donors supporting growth and electroactivity of Geobacter sulfurreducens anode biofilms*. Applied and Environmental Microbiology, vol. 78, pp. 437-444.

[4] Logan B. E., Hamelers B., Rozendal R., Schroder U., Keller J., Freguia S., Aelterman P., Verstraete W., and Rabaey K., (2006). *Microbial Fuel Cells: Methodology and Technology*. Environmental Science and Technology, vol. 40, no. 17.

[5] Fuel Cell Handbook, (2005). *National Energy Technology Laboratory U.S. Department of Energy*. Consulted on-line on July 29 2011.

[6] University of Cambridge, *http://www.ceb.cam.ac.uk/research/groups/rg-eme/teaching-notes/fuelcells*.

[7] Haile S. M., (2003). *Fuel Cell Materials And Components*. Acta Materialia, vol. 51, issue 19, pp. 5981-6000.

[8] Bockris J. O'M., and Srinivasan S., (1969). *Fuel Cells: Their Electrochemistry*. McGraw-Hill, Toronto, Canada.

[9] Bourdakos N., (2012). *Construction and Characterization of Microbial Fuel Cells Using a Defined Co-culture of G. sulfurreducens and E. coli*. MSc Thesis, University of Toronto, Canada.

[10] Reguera G., (2006). *Biofilm and nanowire production lead to increased current in microbial fuel cells*. Applied and Environmental Microbiology, vol. 72, pp. 7345-7348.

[11] Eddy M. (2003). *Wastewater Engineering: Treatment and Reuse*. Fourth edition, McGraw-Hill Science/Engineering/Math, New York, NY, USA.

[12] Larminie J., and Dicks A., (2003). *Fuel Cell Systems Explained*. Second edition, John Wiley and Sons, Ltd.

[13] Butt J. B., (2000). *Reaction Kinetics and Reactor Design*. Second edition, CRC Press.

[14] Panikov N. S., (1995). *Microbial Growth Kinetics*. Springer.

[15] Rhodes P. M., and Stanbury P. F., (1997). *Applied Microbial Physiology: A Practical Approach*. First edition, IRL Press at Oxford University Press.

[16] Rittmann, B. E., and McCarty P. L., (2001). *Environmental Biotechnology: Principles and Applications*. McGraw-Hill Series in Water Resources and Environmental Engineering, Boston, MA, USA.

[17] Reguera G., McCarthy K. D., Mehta T., Nicoll J. S., Tuominen M. T., and Lovely D. R., (2005). *Extracellular electron transfer via microbial nanowires*. Naure, vol. 435, pp. 1098-1101.

[18] Logan B. E., (2008). *Microbial Fuel Cells*. John Wiley and Sons Inc., Hoboken, NJ, USA.

[19] Logan B. E., (2010). *Scaling up microbial fuel cells and other bioelectrochemical systems*. Applied Microbiology and Biotechnology, vol. 85, pp. 1665-1671.

[20] Ahn Y., Ivanov I., Nagaiah T. C., Bordoloi A., and Logan B. E., (2014). *Mesoporous nitrogen-rich carbon materials as cathode catalysts in microbial fuel cells*. Journal of Power Sources, vol. 269, pp. 212-215.

[21] Pant D., Bogaert G. V., Diels L., and Vanbroekhoven K., (2010). *A review of the substrates used in microbial fuel cells (MFCs) for sustainable energy production*. Bioresource Technology, vol. 101, issue 6, pp. 1533-1543.

[22] Ahn Y., Hatzell M. C., Zhang F., and Logan B. E., (2014). *Different electrode configurations to optimize performance of multielectrode microbial fuel cells for generating power or treating domestic wastewater*. Journal of Power Sources, vol. 249, pp. 440-445.

[23] Cheng S., and Logan B. E., (2011). *Increasing power generation for scaling up single-chamber air cathode microbial fuel cells*. Bioresource Technology, vol. 102, issue 6, pp. 4468-4473.

[24] Cheng S., Liu H., and Logan B. E., (2006). *Increased performance of single-chamber microbial fuel cells using an improved cathode structure*. Electrochemistry Communications, vol. 8, pp. 489-494.

[25] Wikipedia, (2015). *Microbial fuel cell*. https://en.wikipedia.org/wiki/Microbial_fuel_cell.

[26] Wikipedia, (2015). *Exoelectrogen*. https://en.wikipedia.org/wiki/Exoelectrogen

[27] Wikipedia, (2015). *Fossil fuel*. https://en.wikipedia.org/wiki/Fossil_fuel

[28] Kapadia A., Nath N., Burg T. C., and Dawson D. M. (2010). *Lyapunov-based continuous stirred tank bioreactor control to maximize biomass production using the monod specific growth model*. American Control Conference Marriott Waterfront, Baltimore, MD, USA.

[29] Shimizu K., (2006). *An overview on the control system design of bioreactors*. Measurement and Control, vol. 50, no. 1, pp. 65 - 84.

[30] Leenheer P. D., and Smith H., (2003). *Feedback control for chemostat models*. Journal of Mathematical Biology, vol. 46, issue 1, pp. 48-70.

[31] Simeonov I., and Diop S., (2010). *Stability analysis of some nonlinear anaerobic digestion models*. International Journal Bioautomation, vol 14, issue 1, pp. 37-48.

[32] Pullammanappallil P. C., Svoronos S. A., Chynoweth D. P., and Lyberatos G., (1998). *Expert system for control of anaerobic digesters*. Biotechnology and Bioengineering, vol. 58, no. 1.

[33] Feng Y., Yang Q., Wang X., and Logan B. E., (2010). *Treatment of carbon fiber brush anodes for improving power generation in air-cathode microbial fuel cells*. Journal of Power Sources, vol. 195, issue 7, pp. 1841-1844.

[34] Nise N. S., (2010). *Control systems engineering*. Sixth edition, Binder Ready Version edition, Wiley, USA.

[35] Marcus A. K., Torres C. I., and Rittmann B. E., (2007). *Conduction based modeling of the biofilm anode of a microbial fuel cell*. Biotechnology and Bioengineering, Wiley InterScience, vol 98, pp. 1171-1182.

[36] Bard A. J., and Faulkner L. R., (2001). *Electrochemical methods: Fundamentals and applications*. John Wiley and Sons Inc., NY, USA.

[37] Torres C. I., Marcus A. K., Lee H. S., Parameswaran P., Brown R. K., and Rittmann B. E., (2010). *A kinetic perspective on extracellular electron transfer by anode-respiring bacteria*. FEMS Microbiology Reviews, vol. 34, pp. 3-17.

[38] Yan M., and Fan L., (2012). *Constant voltage output in two-chamber microbial fuel cell under fuzzy PID control*. International Journal of Electrochemical Science, vol. 8 pp. 3321-3332.

[39] Pinto R. P., (2011). *Dynamic modelling and optimisation of microbial fuel cells and microbial electrolysis cells*. PhD Thesis, cole Polytechnique De Montreal, Canada.

[40] Ahn Y., and Logan B. E., (2012). *A multi-electrode continuous flow microbial fuel cell with seperator electrode assembly design*. Bioenergy and Biofuels, vol. 93, pp. 2241-2248.

[41] Du F., Xie B., Dong W., Jia B., Dong K., and Liu H., (2011). *Continuous flowing membraneless microbial fuel cells with separated electrode chambers*. Bioresource Technology, vol. 102, pp. 8914-8920.

[42] Du Z., Li H., and Gu T., (2007). *A state of the art review on microbial fuel cells: A promising technology for wastewater treatment and bioenergy*. Biotechnology Advances, vol. 25, issue 5, pp. 464-482.

[43] Szederkenyi G., Kristensen N. R., Hangos K. M., and Jorgensen S. B., (2002). *Nonlinear analysis and control of a continuous fermentation process*. Computers and Chemical Engineering, vol. 26, pp. 659-670.

[44] Middaugh J., Cheng S., Liu W., and Wagner R., (2008). *How to make cathodes with a diffusion layer for single-chamber microbial fuel cells* . Pennsylvania State University, USA.

[45] Fan L., Zhang J., and Shi X., (2015). *Performance improvement of a microbial fuel cell based on model predictive control*. International Journal of Electrochemical Science, vol. 10, pp. 737-748.

[46] Zhang X., He W., Ren L., Stager J., Evans P. J., and Logan B. E., (2015). *COD removal characteristics in air-cathode microbial fuel cells*. Bioresource Technology, vol. 176, pp. 23-31.

[47] Cristian P., Katuri K. P., Head I. M., van Loosdrecht M. C. M., and Scott K., (2008). *Mathematical model for microbial fuel cells with anodic biofilms and anaerobic digestion*. Water Science and Technology.

[48] Cristian P., Head I. M., Katuri K. P., van Loosdrecht M. C. M., and Scott K., (2007). *A computational model for biofilm-based microbial fuel cells*. Water Research, vol. 41, pp. 2921-2940.

[49] Noren D. A., and Hoffman M. A., (2005). *Clarifying the butler-volmer equation and related approximations for calculating activation losses in solid oxide fuel cell models*. Journal of Power Sources, vol. 152, pp. 175-181.

[50] Woodward L., Perrier M., Srinivasan B., and Tartakovsky B., (2009). *Maximizing power production in a stack of microbial fuel cells using multiunit optimization method*. Biotechnology Progress, vol. 25, issue 3, pp. 676-682.

[51] Bonnet B., Dochain D., and Steyer J.-P. (1997). *Dynamical modelling of an anaerobic digestion fluidized bed reactor*. Water Science and Technology, vol. 36, issue 5, pp. 285-292.

[52] Wanner O., and Gujer W. (1985). *Competition in biofilms*. Water Science and Technology, vol. 17 (2-3 -3 pt 1), pp. 27-44.

[53] Ljung L., (1999). *System identification: Theory for the user*. Second edition, New Jersey: Prentice-Hall Inc.

[54] Fan Y., Sharbrough E., and Liu H. (2008). *Quantification of the internal resistance distribution of microbial fuel cells*. Environmental Science and Technology, vol. 42, issue 21, pp. 8101-8107.

[55] Logan B., Cheng S., Watson V., and Estadt G., (2007). *Graphite fiber brush anodes for increased power production in air-cathode microbial fuel cells*. Environmental Science and Technology, vol. 41, isue 9, p. 3341-3346.

[56] Buffiere P., Steyer J.-P., Fonade C., and Moletta R. (1995). *Comprehensive modeling of methanogenic biofilms in fluidized bed systems: Mass transfer limitations and multisubstrate aspects*. Biotechnology and Bioengineering, vol. 48, issue 6, pp. 725-736.

[57] B. W. Bequette., (1998). *Process dynamics: Modeling, analysis, and simulation*. Prentice Hall, Upper Saddle River, NJ.

[58] Batstone D. J., Keller J., Angelidaki I., Kalyuzhnyi S. V., Pavlostathis S. G., and Rozzi A., (2002a). *Anaerobic digestion model no 1 (ADM1): IWA Publishing*. London, UK.

[59] Keesman K. J., and Stgtr J. D., (2003). *Optimal input design for low-dimensional systems: an haldane kinetics example*. European Control Conference, The Netherlands.

[60] O'Hayre R., Cha S.-W., Colella W., and Prinz F. B. (2006). *Fuel cell fundamentals*. First edition, Hoboken, N.J. : John Wiley and Sons.

[61] Mailleret L., Bernard O., and Steyer J. P., (2004). *Robust regulation of anaerobic digestion processes*. Water Science and Technology, vol. 48 no 6, pp. 87-94.

[62] Mailleret L., Bernard O., and Steyer J. P., (2004). *Nonlinear adaptive control for bioreactors with unknown kinetics*. Automatica, vol. 40, pp. 1379-1385.

[63] Karafyllis I., Kravaris C., Syrou L., and Lyberatos G., (2008). *A vector lyapunov function characterization of input-to-state stability with application to robust global stabilization of the chemostat*. European Journal of Control, vol. 1, pp. 47-61.

[64] Moat A. G., Foster J. W., and Spector M. P., (2002). *Microbial physiology*. Fourth edition, Wiley-Liss, Inc., NY, USA.

[65] Lanas V., and Logan B. E., (2013). *Evaluation of multi-brush anode systems in microbial fuel cells*. Bioresource Technology, vol. 148, pp. 379-385.

[66] D'ans G., Gottlieb D., and Kokotovic P., (1972). *Optimal control of bacterial growth*. Automatica, vol. 8, pp. 729-736.

[67] Bayen T. Mairet F., and Mazade M., (2010). *Optimal feeding strategy for the minimal time problem of a fed-batch bioreacor with mortality rate*. John Wiley and Sons, Ltd.

[68] Ashoori A., moshiri B., Khaki-Sedigh A., and Bakhtiari M. R., (2009). *Optimal control of a nonlinear fed-batch fermentation process using model predictive approach*. Journal of Process Control, vol. 19, pp. 1162-1173.

[69] Yamamoto S., Suzuki K., Araki ., Mochihara H., Hosokawa T., Kuboa H., Chiba Y., Rubab O., Tashiro Y., and Futamata H., (2014). *Dynamics of different bacterial communities are capable of generating sustainable electricity from microbial fuel cells with organic waste*. Microbes and Environments, vol. 29, issue 2, pp. 145-153.

[70] Huang L., Cheng S., Rezaei F., and Logan B. E., (2009). *Reducing organic loads in wastewater effluents from paper recycling plants using microbial fuel cells*, Environmental Technology, vol. 30, issue 5, pp. 499-504.